Interaction of XMAP215 with a microtubule plus-end studied with optical tweezers

Dissertation

zur Erlangung des akademischen Grades
Doctor rerum naturalium
(Dr. rer. nat.)

vorgelegt
der Fakultät Mathematik und Naturwissenschaften
der Technischen Universität Dresden

von

Anastasiya V. Trushko

geboren am 28. April 1984
in Minsk, Weißrussland

Dresden, December 2011

Interaction of XMAP215 with a Microtubule Plus-end Studied with Optical Tweezers
Anastasiya Trushko, PhD thesis, TU-Dresden, December 2011.

Supervisors:

Prof. Dr. Jonathon Howard

Max Planck Institute of Molecular Cell Biology and Genetics (MPI-CBG)
Pfotenhauerstrasse 108, 01307 Dresden, Germany

Dr. Erik Schäffer

Nanomechanics group, Biotechnology Center (BIOTEC),TU-Dresden Tatzberg 47-51, 01307 Dresden, Germany

Thesis Advisory Committee:

Prof. Dr. Petra Schwille

Biotechnology Center (BIOTEC),TU-Dresden Tatzberg 47-51, 01307 Dresden, Germany

Dr. Iva Tolic-Norrelykke

Max Planck Institute of Molecular Cell Biology and Genetics (MPI-CBG)
Pfotenhauerstrasse 108, 01307 Dresden, Germany

This thesis was reviewed by:

Prof. Dr. Jonathon Howard

Prof. Dr. Robert Cross

The work described in this thesis was performed at Prof. Dr. Jonathon Howard group, Max Planck Institute of Molecular Cell Biology and Genetics, Pfotenhauerstrasse 108, 01307 Dresden, Germany

The author was enrolled in Technical University of Dresden

The author was enrolled in the PhD program of Dresden International Graduate School for Biomedicine and Bioengineering.

To my mother

Abstract

Microtubules are a part of the cell cytoskeleton that performs different functions, such as providing the mechanical support for the shape of a cell, acting as tracks along which the motor protein move organelles from one part of the cell to another, or the forming mitotic spindle during the cell division. The microtubules are dynamic structures, namely they can grow and shrink. The phase of microtubule growth alternates with the phase of shrinkage that results in the dynamic microtubule network in the cell. However, to form stable and spatially well-defined structures, such as a mitotic spindle, the cell needs to control this stochastic process. This is done by microtubule associated proteins (MAPs). One class of MAPs is the proteins of XMAP216/Dis1 family, which are microtubule polymerases. The founding member of this family is *X. laevis* XMAP215.

XMAP215 is a processive polymerase acting on the microtubule plus end. XMAP215 binds either directly or reaches the microtubule plus end by the diffusion along the microtubule lattice. Being at the microtubule plus-end XMAP215 stays there transiently and helps to incorporate up to 25 tubulin dimers into microtubule lattice before it dissociates and, therefore, it processively tracks the growing microtubule end during polymerization. There are two hypothesis of microtubule assembly promotion: (i) XMAP215 repeatedly releases an associated tubulin dimer into the microtubule growing plus end or (ii) structurally stabilizes a polymerized tubulin intermediate at the growing plus end and, therefore, preventing depolymerization events. The first way results into the increase of on-rate of tubulin dimers at the microtubule end, whereas the second way results into the decrease of off-rate of tubulin dimers at the microtubule end.

Here, I show the study of the mechanism of microtubule growth acceleration by XMAP215 and the dependence of XMAP215 polymerization activity on the applied force. To answer these questions, I investigated the addition of tubulin dimers to the plus end of the microtubule by XMAP215 and how this addition depends on the applied force. XMAP215 remains at the microtubule end for several rounds of tubulin addition surfing both growing and shrinking microtubule ends. Therefore, if one could track the position of the XMAP215 molecules at the very tip of a microtubule with sufficient resolution, it would provide the information about the dynamics of the microtubule end. The technique, which can detect the position of the object of interest with high spatial and temporal resolution in addition to being able to exert a force, is an optical trap. A calibrated optical trap not only provides a good measure of displacement but also enables force measurements. To monitor the position of the molecules of interest, the molecules of interest are usually attached to a microsphere. Hence, I tethered XMAP215 to a microsphere held by an optical trap, and used XMAP215 as a handle to interact with the microtubule tip. When the microtubule grows, the XMAP215 coated microsphere will move in the optical trap and this movement can be detected with high temporal and spatial resolution.

My work demonstrates that cooperatively working XMAP215 molecules can not only polymerize microtubule but also harness the energy of microtubule polymerization or depolymerization to transport some cargo. There is an evidence that orthologues of XMAP215 in budding yeasts, fission yeasts and *Drosophila* localize on the kinetochores. Therefore, the ability of the bearing some load during microtubule polymerization could be potentially important for the XMAP215 functioning during cell division.

I also showed the influence of external force applied to the XMAP215 molecules. Pointing toward microtubule growth, a force of 0.5 pN applied to the microtubule tip-coupled XMAP215-coated microsphere increases XMAP215 polymerization activity. However, the force of the same magnitude but applied against microtubule growth does not affect XMAP215 polymerization activity. This result can be explained by the fact, that the force acting in the direction of microtubule growth constrains XMAP215 to be at the very microtubule tip. Hence, XMAP215 can not diffuse away from plus-end and there is higher chance to incorporate tubulin dimers into the microtubule plus-end. The on- and off-rate of tubulin dimers at the microtubule end are both decreased when the external force applied either in direction of microtubule growth or opposite to it. The external force affects the off-rate slightly stronger than on-rate of tubulin dimer. Taking together, my study gives new insights into the mechanism of microtubule polymerization by XMAP215 and show some novel properties of this protein.

Contents

Chapter 1

Introduction

1.1 Microtubules form different cellular structures to perform their functions in a cell

Microtubules are a part of the eukaryotic cytoskeleton. They are long polymers in a shape of hollow tubes, which form different structures in the cell. In the animal cell microtubules grow out of an organizing center, the *centrosome*. When a cell does not divide the microtubules form a network, which provides anchoring for the organelles in certain cell regions and also serves as a system of tracks for the intracellular trafficking. These microtubules can assemble and disassemble quickly to rearrange the whole microtubule network. When the cell starts to divide the microtubules are reorganized into a special structure called the *mitotic spindle*, which pulls apart the chromosomes and segregates them equally into two daughter cells. Microtubules can form also stable structures such as *cilia* and *flagella*. These appear on the cell surface as hair-like structures that beat rhythmically. They serve for the movement of the cells or sweeping fluid over the cell surface.

1.2 Microtubule Structure and Dynamics

As it was mentioned above, microtubules are involved in a variety of cellular processes. To fulfill these rather different functions the microtubule network, also called the *microtubule cytoskeleton*, has to be able to rearrange itself in size and shape. Moreover, this has to happen over a short time. To understand how this microtubule network rearrangement occurs, one needs to understand the structure and properties of a single microtubule.

1.2.1 Microtubules are Polymers Consisting of Tubulin Dimers

Microtubules are polymers consisting of tubulin heterodimers. The tubulin heterodimers consist of globular α- and β-tubulin subunits (Fig.1.1 (A)). They have the molecular mass of $\sim$ 100 kDa and are 8 nm long. The microtubules assemble by addition of the

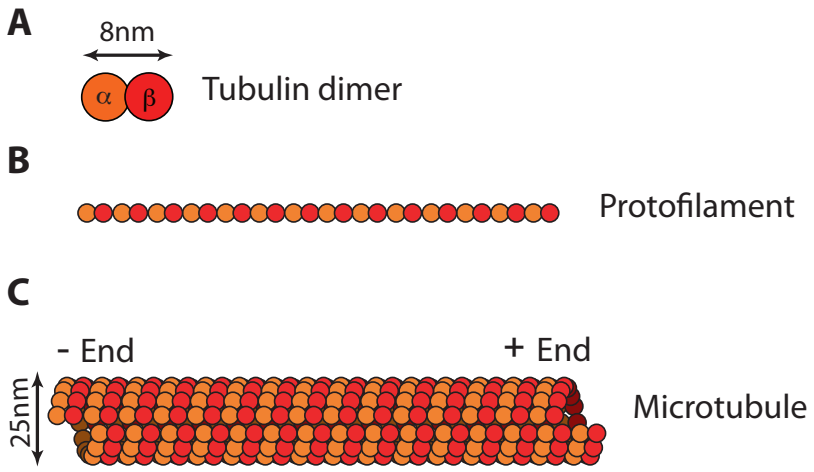

Figure 1.1: Microtubule structure. A. Tubulin dimer consist of α- and β- tubulin subunits. **B.** Tubulin dimers are sticking to each other in the head-to-tail manner and form a protofilament. Because of such arrangement of tubulin dimers, each protofilament has a polarity: one end capped by α- tubulin and other by β- tubulin subunit. **C.** The cylindrical and helical microtubule wall typically is formed by 13 parallel protofilaments. Because of the parallel arrangement the whole microtubule has a polarity: at one end α- tubulin subunits are exposed and at other β- tubulin subunits.

$\alpha\beta$-tubulin heterodimers at either end and disassemble by loss of them. The tubulin dimers stick to each other in a head-to-tail manner and form a *protofilament* (Fig.1.1 (B)). Because of such an arrangement of tubulin dimers, the whole protofilament has a polarity: at one end the α- tubulin subunit is exposed and at the other the β- tubulin subunit. The protofilaments form the wall of the microtubule. The number of the protofilaments in the microtubule wall varies from 10 to 15, but the most common number in the cell is 13, which sets the microtubule diameter to 25 nm (Fig.1.1 (C)). All protofilaments are oriented in the same fashion in the microtubule wall. This gives the polarity to the whole microtubules with one end capped with α-tubulin subunits and the other end with β-tubulin subunits. The latter end grows faster *in vitro* and is named *plus end*, the other, slower growing, is the *minus end*. In the animal cell, the microtubule minus ends are embedded into organizing center called *centrosome* and the plus ends are exposed to the cytosol. In yeasts, the assembling structure is the *spindle pole body*.

1.2.2 Microtubules are Dynamic Structures

Microtubules are dynamic structures. *In vivo* they grow slowly and then abruptly shrink quickly. The phase of growth alternates with the phase of shrinkage continuously. This behavior is called *dynamic instability* [84]. The switch between the microtubule growth

to the shrinkage is called a *catastrophe event* and the switch between the microtubule shrinkage back to the growth is a *rescue event* (Fig.1.2 (B)).

1.2.3 Microtubule dynamic instability is coupled to the GTP hydrolysis

Dynamic instability arises from the intrinsic property of the tubulin protein and it can be easily reconstituted in vitro by mixing guanosine triphosphate (GTP) nucleotide and tubulin molecules in the presence of the nucleating centers. The dynamic instability is a result of the capability of tubulin dimers to hydrolyze GTP to guanosine diphosphate (GDP).

Each α- and β-tubulin monomer binds one GTP nucleotide. The one bound to the α-tubulin is positioned at the interface of α-β monomers and is non-exchangeable and non-hydrolyzable. The other, bound to the β- tubulin, is accessible for hydrolysis and can be exchanged. The GTPase activity of a free tubulin dimer is very low, but it can be stimulated by binding to other tubulin dimers. When another tubulin dimer is bound, the necessary residues for the hydrolysis are provided by the new α-tubulin subunit and the exposed GTP nucleotide on the β-tubulin surface is hydrolyzed to the GDP. Therefore, when a microtubule is built up by the tubulin dimers binding at either of its end, most of the tubulin dimers contain GDP. Only the tubulin dimers at the leading edge of the microtubule have still GTP nucleotides. If the addition of tubulin dimers to the microtubule end is faster then the GTP hydrolysis rate, the layer of the GTP containing tubulin dimers will grow, forming a so-called *GTP cap* (Fig.1.2 (B)).

The hydrolysis of GTP affects the structure of the tubulin dimer. The tubulin dimer containing the GDP nucleotide experiences a mechanical strain that leads to a kink in the α-β- tubulin interface, when the GTP containing tubulin dimer remains straight (Fig.1.2 (A)). This change in tubulin dimer structure, in turn, gives the curved shape to the whole protofilament. In the microtubule lattice, however, the protofilaments are forced to be straight by the lateral bonds between them. And they are additionally stabilized by the GTP cap. When the GTP cap is lost because of the hydrolysis or other depolymerizing factors, the protofilaments start to curve at the ends and the microtubule undergoes depolymerization releasing the stored energy of mechanical strain.

1.2.4 Dynamic microtubules exert forces and move the cellular structures

Due to the dynamic instability of the microtubules a cell can quickly rearrange its microtubule network. This is crucial for the formation of differently, spatially organized structures from the same tubulin pool. Furthermore, rapidly assembling and disassembling microtubules can perform a three-dimensional search in the cytosol, which is important, for example, for the kinetochore capturing of the chromosomes by the microtubule plus tips during the cell division. When interacting with cellular structures,

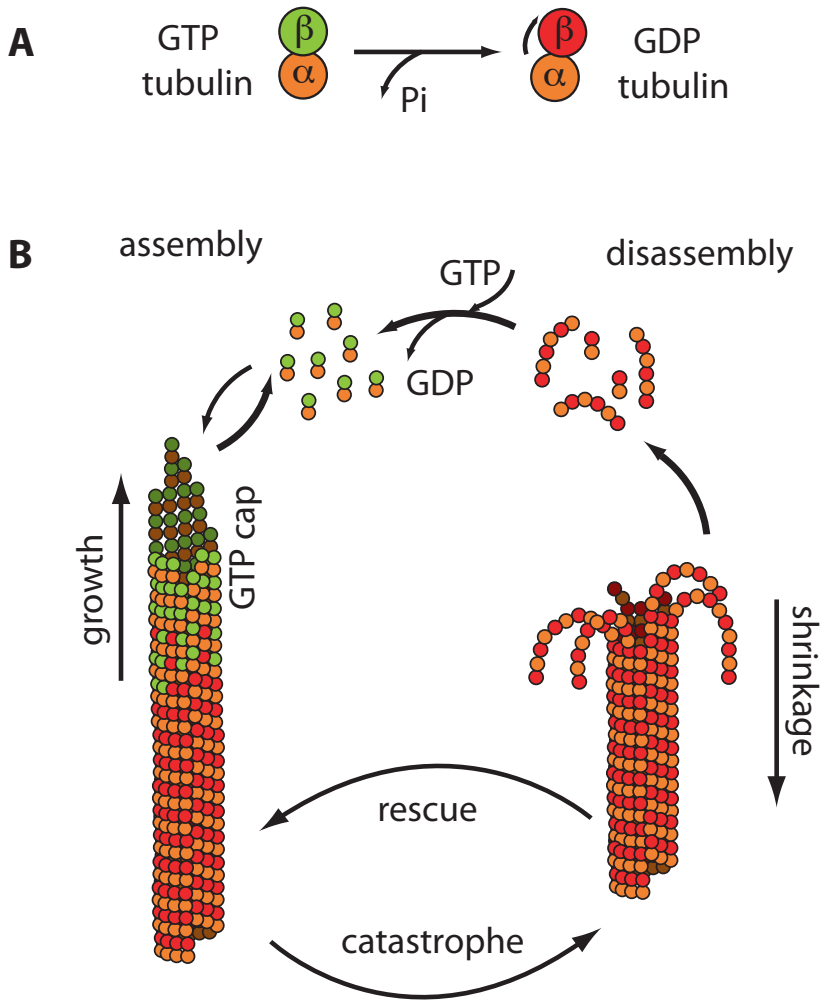

Figure 1.2: Microtubule assembly and disassembly. A. Conformational change of tubulin dimer accompanying GTP hydrolysis. **B.** Microtubule dynamic instability. Polymerization is typically initiated from the pool of GTP-containing tubulin. Many GTP-tubulin dimers encounter the growing microtubule tip, however, only a small fraction of them are incorporated into the microtubule wall. Shortly after incorporation, the GTP of a β-tubulin subunit gets hydrolyzed to GDP. This induces a kink in the tubulin dimer. Because the tubulin dimers are aligned in the protofilament, the latter will also get curled if the containing tubulin dimers have bound GDP. However, the protofilaments are forced to be straight in the microtubule wall and additionally stabilized by the GTP cap. During microtubule assembly, microtubule plus-ends form a sheet-like structure [30][75]. Once the GTP cap is lost the protofilaments peel off and the microtubule undergoes a catastrophe, releasing GDP-tubulin dimers. The assembly-disassembly cycle is completed by exchanging GDP of the disassembly products with GTP.

the dynamic microtubules can exert forces, pushing when they assemble and pulling when they disassemble (rev. [54, 39]). Because of these forces, microtubules can move cellular structures inside the cell if the attachments is maintained during their growth and shrinkage. In such a way, during the cell division, after establishing the chromosome attachments to the microtubule tips via the kinetochores, the chromosomes are moved either towards or away from the spindle pole, following the shrinking or growing microtubule tip respectively [31, 58].

Other examples are the movement of the nucleus or the mitotic spindle because of the interaction of the microtubules and the cell cortex. Thus, for example, in the fission yeast *S. pombe*, microtubules attach to the nucleus via spindle pole bodies. They grow against the cell cortex and exert pushing forces on the nucleus from both sides and center it [117, 34]. In budding yeasts *S. cerevisiae*, after the formation of the mitotic spindle, the microtubules grow out of the spindle poles and enter the bud. Upon attachment to the bud cortex the microtubule start to depolymerize maintaining attachment and pull the mitotic spindle towards the bud. Because of these pulling forces, the mitotic spindle is properly centered between the mother and daughter cell [71, 129].

In vitro studies with purified tubulin confirmed that the polymerizing and depolymerizing microtubule end can exert pushing and pulling forces, respectively [37, 72]. Thus, the assembling microtubules can deform the membranes or induce microtubule buckling. And the disassembling or assembling microtubule tip can move a microsphere attached to it [49, 10, 96, 41].

1.3 Factors Regulating Microtubule Dynamics

Due to the dynamic instability, a cell can quickly rearrange its microtubule network. However, the dynamic instability is a stochastic process, and to form stable and spatially well-defined structures, such as a mitotic spindle, the cell needs to tightly regulate both the microtubule assembly and their disassembly. This regulation is done by microtubule associated proteins (MAPs) that falls into several classes: microtubule assembly promoters, disassembly promoters, and stabilizers [55, 1, 4].

Microtubule dynamic instability can be characterized by four parameters: microtubule growth speed, microtubule shrinkage speed, frequency of the rescue events, also called rescue rate, and frequency of the catastrophe events, catastrophe rate. Most of the MAPs that modulate microtubule dynamics alter one or several of these parameters. Thus, the assembly promoting factors may suppress microtubule catastrophes or favor microtubule rescues, increase growth speed and decrease shrinkage speed. The microtubule destabilizing factors, on the contrary, may decrease growth speed and increase shrinkage speed, as well as facilitate catastrophes and prevent rescues events (Fig.1.3).

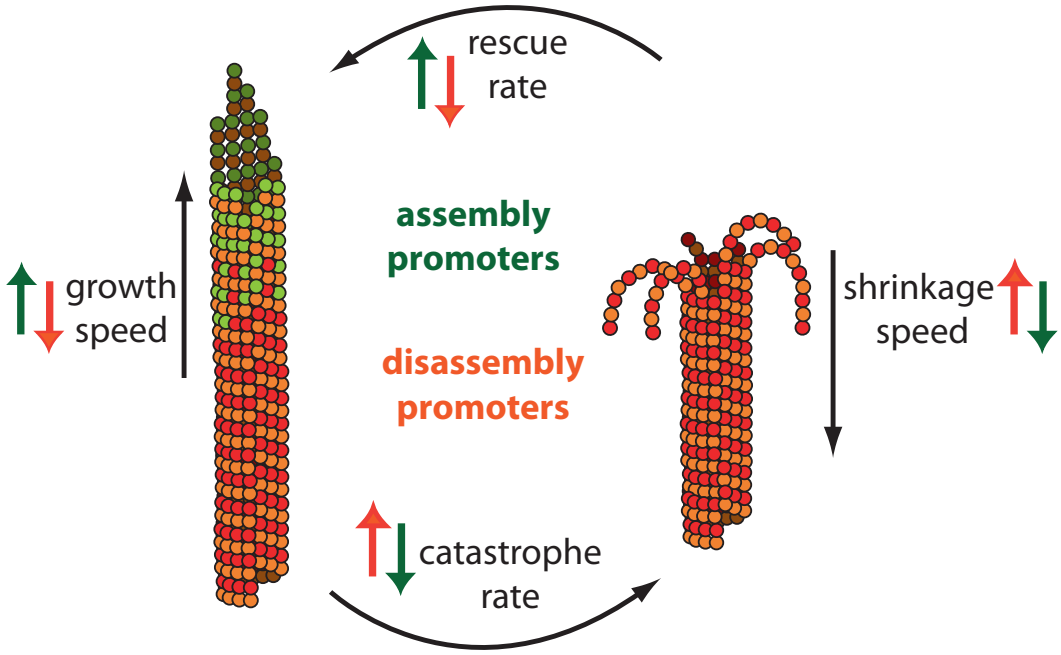

Figure 1.3: Microtubule Dynamic Instability is regulated by assembly and disassembly promoters. The microtubule dynamic instability can be described by four parameters: growth speed, shrinkage speed, catastrophe rate and rescue rate. Assembly promoters suppress microtubule catastrophes and decrease shrinkage speed (denoted by green arrows pointing downwards), favor microtubule rescues and increase growth speed (denoted by green arrows pointing upwards). Disassembly promoters decrease growth speed and prevent rescue events (denoted by orange arrows pointing downwards), and increase shrinkage speed, as well as facilitate catastrophes (denoted by orange arrows pointing upwards).

1.3.1 Microtubule Disassembly Promoters

In opposition to the assembly promoters, microtubule disassembly promoters induce microtubule catastrophes, promote disassembly, and inhibit depolymerization. They are represented by proteins of kinesin-8, kinesin-13, kinesin-14, and Op18/Stathmin families.

The kinesin-8 motors are depolymerases destabilizing microtubules exclusively from the microtubule plus-end [50, 121], whereas proteins of the kinesin-13 family destabilize microtubules from both plus-end and minus-end [52, 35, 82, 128, 85]. The kinesin-8 proteins reach the plus-end by directed movement along the microtubule lattice powered by adenosine triphosphate (ATP) hydrolysis. Once at the microtubule plus-end, kinesin-8 proteins depolymerize the microtubules in a length-dependent manner [121, 114]. Kinesin-13 proteins get to the microtubule ends by one-dimensional diffusion over the microtubule lattice [52]. However, kinesin-13 needs ATP hydrolysis to curl out the mi-

crotubule protofilaments and induce their depolymerization [57, 42, 91]. Some proteins of the kinesin-14 family, *S. cerevisiae* Kar3, *D. melanogaster* Ncd, and *S. pombe* Klp2, have depolymerization activity, however, it remains unclear whether the depolymerization activity is conserved for all family members [109, 118].

In contrast to kinesins, the proteins of the Op18/Stathmin family do not use the energy of ATP hydrolysis to induce microtubule catastrophes. Stathmin, the founding member of the family, promotes microtubule depolymerization in two ways. One is by sequestration of tubulin via binding to it and forming a complex that is not able to bind to the microtubule end [62, 15, 33, 73, 110, 98]. The second way is the direct binding to the microtubule plus-end and kinking the tubulin dimer at the microtubule tip; this makes the microtubule undergo catastrophe [15, 56, 126, 81].

1.3.2 Microtubule Stabilizers

Microtubule stabilizers are represented by proteins of the MAP1, MAP2/Tau and Doublecortin families. These proteins are mainly expressed in neurons where long stable microtubules are essential for proper neuronal functions. The proteins of these families do not interact with the microtubule plus-end, but rather bind along the microtubule lattice. The MAP1 and MAP2/Tau proteins are known to stabilize microtubules and reduce their depolymerization rate by binding along the microtubule lattice and reinforce longitudinal bonds between tubulin dimers [120, 97, 66, 26]. Doublecortin favors 13-protofilament microtubules and binds between the protofilaments stabilizing the longitudinal bonds between tubulin dimers [86]. It decreases catastrophe rate, although it does not affect microtubule growth rate [86, 87].

1.3.3 Microtubule Assembly Promoters

Microtubule assembly promoters are represented by XMAP215/Dis1 proteins, end binding proteins (EBs), cytoplasmic linker proteins (CLIPs), Cytoplasmic linker associated proteins (CLASPs), and adenomatous polyposis coli (APC). All these proteins preferentially localize at microtubule plus-end. Because of this ability, they are also called *+TIPs*. Associated with the plus-end, all these proteins modulate different parameters of the microtubule growth to promote the microtubule assembly.

For example, XMAP215/Dis1 proteins are shown to increase the microtubule growth rate, whereas EBs mainly function as a platform for binding other MAPs modulating microtubule dynamic instability such as APC, kinesin-13 (MCAK), CLIPs, CLASPs and etc [3, 61]. There is some evidence that EBs also inhibit catastrophes, promote rescues, and stimulate the microtubule growth rate on its own. However, the results of studies of EB modulation of microtubule dynamics directly are controversial and vary between different experimental systems. In *Saccharomyces cerevisiae* and in cultured *Drosophila* cells EB1 increases both catastrophes and rescues [113, 101, 127]. In *Xenopus* extracts

EB1 stimulates microtubule growth, facilitates rescues and inhibits catastrophes [112]. In *Schizosaccharomyces pombe*, EB1 also inhibits catastrophes and promotes the initiation of microtubule growth [24]. However, *in vitro* studies of EB1and Mal3 effect on microtubule dynamics polymerized from purified tubulin suggest that these proteins facilitate not only rescues but also catastrophes [17, 122], although another *in vitro* studies of microtubule dynamics showed catastrophe suppression by EB1 [80] and no effect of EB1 on the catastrophes was observed in [36].

CLIPs are thought to be factors promoting microtubule rescues. CLIPs localize during interphase at microtubule plus tips [95] and on microtubule lattice in "patches" [99] and during prometaphase at the kinetochores [38]. *In vivo* in fission yeast [23] and in budding yeast [16], as well as in mammals [70] CLIPs were shown to be the factors promoting microtubule rescues. *In vitro* studies of interaction of dimeric head domain of CLIP170 with dynamic microtubules grown from purified tubulin shows the microtubule rescues promotion [9].

CLASPs not only promote rescues, but also suppress catastrophes and stabilize microtubules [78, 79, 59, 83, 19]. They are recruited to the microtubule plus end by binding to the +TIP proteins EBs and CLIP170 [2, 83]. *In vitro* studies of the fission yeast CLASP, Cls1p, showed that it decreases the frequency of microtubule catastrophes and increases the frequency of microtubule rescues [7]. Cls1p diffuses on the microtubule lattice but can not track the microtubule growing plus end. The microtubule rescue occurs at sites of an accumulation of Cls1p molecules [7].

APC was reported to stabilize microtubules, increase the time of their growth and decrease their shortening time, shrinkage rate and catastrophe frequency [68, 88, 89]. It is a +TIP protein. In interphase it accumulates at the microtubule plus-end as round clusters [90], whereas during mitosis APC localizes to chromosomes at kinetochore-microtubule attachment sites [40, 63, 48]. APC interacts with EB1 that facilitates APC localization on the growing microtubule plus-end (Su 1995), although APC can bind to the microtubule plus-end directly [107, 130].

In the following section I describe the structure, localization, functions and influence on microtubule dynamics of the XMAP215 protein since it is the protein of my study.

1.4 XMAP215/Dis1 proteins catalyze microtubule growth

Family members. XMAP215/Dis1 proteins promote microtubule assembly by increasing microtubule growth speed. The members of this family include *H. sapiens* chTOG [29], *D. melanogaster* Msps [32], *C. elegans* ZYG9, *X. laevis* XMAP215 [44], *A. thaliana* MOR1 [124], *S. cerevisiae* Stu2 [123] and *S. pombe* Dis1 [100], Alp14 [43].

Localization and functions *in vivo*. The proteins of XMAP215/Dis1 family localize at the microtubule plus ends and to varying degrees along the microtubule lattice, centrosomes, and kinetochores. The loss of functions of this protein in a cell leads to short interphase microtubules because of their reduced growth speed and increased frequencies of catastrophe and pause events [43, 32, 123, 116, 21, 64]. In mitotic cells, the disruption of the XMAP215/Dis1 protein function leads to small, abnormally organized mitotic spindles and short astral microtubules [32, 47, 28]. At the kinetochores, these proteins are required for the regulation of the attachment of microtubule to the kinetochores [43, 111]. In budding yeasts, Stu2 mediates formation of microtubules at the kinetochores, which are attached afterwards to the mitotic spindle [69]. This facilitates correct attachment of the chromosomes. At the centrosome in *D. melanogaster* [74], *X. laevis* [67], and *C. elegans* [14], XMAP215/Dis1 proteins are shown to interact with transforming acidic coiled-coil (TACC) proteins and increase the number and the length of the centrosomal microtubules during mitosis. However, it remains unclear whether XMAP215/Dis1 proteins act at the centrosomes as microtubule plus end polymerases or have other functions at the microtubule minus end.

XMAP215 is a processive polymerase. The first identified member of this family was *X. laevis* XMAP215 isolated from egg extracts as a growth promoting factor [44]. It was reported that XMAP215 accelerates the microtubule growth rate tenfold [44]. *In vitro* studies of the interaction of recombinant XMAP215 with purified tubulin showed that oligomers of tubulin are added to the growing plus end of the microtubule both in the presence and absence of XMAP215 [65]. They used an optical trap that held a microsphere attached to a microtubule. The plus end of the microtubule grew against a solid substrate. The growing microtubule pushed the microsphere from the focus of the optical trap. A weakness of the experiment was that the temporal resolution in their experiments was low (25 Hz). Scheck et al. [104] used a similar assay but without the presence of XMAP215. In their experiments, the temporal resolution was higher (5 kHz). They saw no evidence for individual steps that correspond to addition of oligomers. Thus, they argued that the Kerssemakers [65] length variation was not due to a small number of large steps but due to a large number of fast small steps. These fast steps were below the resolution limit with respect to both time and position, which was 10 nm in these experiments. Kerssemakers et al. additionally saw an increase in microtubule growth steps in the presence of XMAP215. They interpreted this as an evidence for a shuttle model. In this model, each XMAP215 chaperons several tubulin dimers to the microtubule end. Slep and Vale proposed a similar model [106].

Evidence from Brouhard et al. [22], however, shows that this model cannot be correct: (i) XMAP215 only binds one tubulin dimer both in solution (by ultracentrifugation and gel filtration studies) and on the microtubule lattice under growth conditions (by single molecule experiments). (ii) The rate of XMAP215 binding to ends is too slow to account for the high growth rates even if it brought several tubulin dimers with it each time it bound to the end. (iii) XMAP215 remains at the end for too long - a shuttle must

rapidly deposit its cargo before going back for more.

Based on their experimental data, Brouhard et al. proposed that XMAP215 is a processive polymerase acting on the microtubule plus end. XMAP215 binds it either directly or reaches the microtubule plus end by the diffusion along the microtubule lattice. Once at the microtubule plus end, XMAP215 stays there transiently and helps to incorporate 25 tubulin dimers into the microtubule lattice before it dissociates and, therefore, it processively tracks the growing microtubule end during polymerization. XMAP215 can promote microtubule assembly either (i) by repeated addition of a tubulin dimer into the microtubule growing plus end or (ii) by structural stabilization of a polymerized tubulin intermediate at the growing plus end and, therefore, prevention of depolymerization events. This model was also recently confirmed by structural analysis of *Xenopus* XMAP215 [125].

XMAP215 also tracks the depolymerizing microtubule end. It was shown *in vitro* that XMAP215 and Stu2 can catalyze the reverse reaction, namely the microtubule depolymerization, at low concentration of tubulin protein added to the GMPCPP-stabilized microtubule seeds [22, 20]. Therefore, XMAP215 and its orthologs are catalysts, which act either as polymerases or depolymerases depending on which reaction direction the experimental conditions favor. However, it remains unclear whether all the members of the XMAP215/Dis1 family are polymerases or have other functions.

Structure of XMAP215/Dis1 proteins. The hallmark of XMAP215/Dis1 family is tumor overexpressed gene (TOG) domains [8, 6]. Depending on the species, the orthologs of this family have different number of TOG domains. For example, *Xenopus* XMAP215, as well as fly Msps, human chTOG and plant MOR1, is monomeric and has five TOG domains, whereas in *C. elegans* ZYG9 is also monomeric but has three TOG domains and budding yeast Stu2 and fission yeast Dis1 are dimeric and each monomer has only two TOG domains. The TOG domain contains a highly conserved α-helical fold consisting of six conserved HEAT repeats that form a paddle-like structure [8]. The TOG domains have high affinity to the soluble tubulin dimer and poorly interact with the microtubule lattice [8, 5, 108, 93]. Each monomeric and dimeric XMAP215/Dis1 protein binds one tubulin dimer at a time [22, 5]. In case of monomeric proteins, namely XMAP215 (Xl), chTOG (Hs), Msps (Dm), the molecule is flexible [27] and wraps around the outer surface of the tubulin dimer [22], while the dimeric proteins Stu2 (Sc) and Dis1 (Sp) clutch the tubulin dimer between TOG domains of two monomers [5].

Recently, it was shown that TOG domains are essential for the *Xenopus* XMAP215 polymerization activity [125]. Upon inactivation of high tubulin affinity TOG1 and TOG2 XMAP215 polymerization activity drops by 75%, whereas inactivation of low-affinity TOG3 and TOG4 results in reduction of 25% of polymerization activity. Although an XMAP215 mutant containing only TOG1 and TOG2 is functional, the polymerization activity of this construct is lower than one of the full-length protein, pointing to the fact

that all XMAP215 TOG domains are necessary for full protein functionality. However, the dimeric yeast proteins Dis1 and Stu2 contain only two pairs of TOG1 and TOG2 domains [119]. A different part of XMAP215 molecule is responsible for the microtubule lattice binding and diffusion. For XMAP215, it is the region between TOG4 and TOG5[125]. This region is positively charged and possibly interacts with the E-hooks of the microtubule. It is called *S/K-rich domain* because it contains the stretches of serine, glycine, and lysine residues [5, 6].

1.5 Motivation of my PhD Thesis

Microtubules are a part of the cell cytoskeleton that perform different functions, such as providing the mechanical support for the shape of the cell, acting as tracks along which the motor protein move organelles from one part of the cell to another, or forming mitotic spindle during the cell division. The microtubules are dynamic structures, namely they can grow and shrink. The phase of microtubule growth alternates with the phase of shrinkage that results in the dynamic microtubule network in the cell. However, to form stable and spatially well-defined structures, such as a mitotic spindle, the cell needs to control this stochastic process. This is done by microtubule associated proteins (MAPs). One class of MAPs is the proteins of XMAP215/Dis1 family, which are microtubule polymerases. The founding member of this family is *X. laevis* XMAP215.

Based on their experimental data, Brouhard et al. [22] proposed that XMAP215 is a processive polymerase acting on the microtubule plus end. XMAP215 binds either directly or reaches the microtubule plus end by diffusion along the microtubule lattice. While at the microtubule plus end, XMAP215 stays there transiently and helps to incorporate 25 tubulin dimers into microtubule lattice before it dissociates and, therefore, it processively tracks the growing microtubule end during polymerization. XMAP215 can promote microtubule assembly either (i) by repeated releasing associated tubulin dimer into the microtubule growing plus end or (ii) by structural stabilization of a polymerized tubulin intermediate at the growing plus end and, therefore, preventing depolymerization events.

The question which I would like to address here is how XMAP215 accelerates microtubule growth. Does it increase the on-rate of tubulin dimers, k_{on}, or decrease off-rate k_{off}? Is the XMAP215 polymerization activity dependent on an applied force? To answer these questions, I need to investigate the addition of tubulin dimers to the plus end of the microtubule by XMAP215 and how this addition depends on the applied force. XMAP215 remains at the microtubule end for several rounds of tubulin addition surfing both growing and shrinking microtubule end [22]. Therefore, if one could track the position of the XMAP215 molecules at the very tip of a microtubule with sufficient resolution, it would provide the information about the dynamics of the microtubule end. The technique, which can detect the position of the object of interest with high spatial and temporal resolution in addition to being able to exert a force, is an optical trap. A

calibrated optical trap not only provides a good measure of displacement but also enables force measurements. To monitor the position of the molecules of interest, the molecules of interest are usually attached to a microsphere. Hence, I tethered XMAP215 to a microsphere held by an optical trap, and used XMAP215 as a handle to interact with the microtubule tip. When the microtubule grows, the XMAP215 coated microsphere will move in the optical trap and this movement can be detected with high temporal and spatial resolution.

Chapter 2

Protein expression, purification and labeling

This chapter provides the description of the procedures of tubulin purification, the labeling with fluorescent dye, as well as the procedures of expression and purification of XMAP215 fused with GFP and His7.

2.1 Tubulin Purification and Labeling

2.1.1 Purification of Tubulin from Porcine Brain

To study the microtubule growth and shrinkage in vitro, one needs to assemble microtubules out of purified heterodimeric $\alpha\beta$- tubulin to reconstitute dynamic microtubules. For this purpose, purified tubulin from porcine brain is used. The purification protocol consists of homogenization of the brains followed by two steps of clarification of the homogenate and cycles of tubulin polymerization in the presence of GTP, centrifugation, and depolymerization [46]. The idea is that the soluble molecules of heterodimeric tubulin within a certain concentration range form microtubules in the presence of GTP. These assembled microtubules can be spun down using high-speed centrifugation and separated from cell membranes and other non-microtubule-associated proteins (non-MAPs). The final solution contains the soluble molecules of heterodimeric $\alpha\beta$-tubulin and microtubule-associated proteins (MAPs). To purify the tubulin protein from MAPs one passes the above mentioned solution through a phosphocellulose (PC) column, in which the MAPs bind and tubulin molecules pass through. Then the purified protein is frozen in liquid nitrogen for long-term storage (Fig. 2.1).

2.1.2 Cycling of Purified Tubulin

Before usage for in vitro studies, the purified porcine tubulin has to undergo a final cycling, the process of additional polymerization, centrifugation, depolymerization of the microtubules. This step ensures the presence of only tubulin that is able to assem-

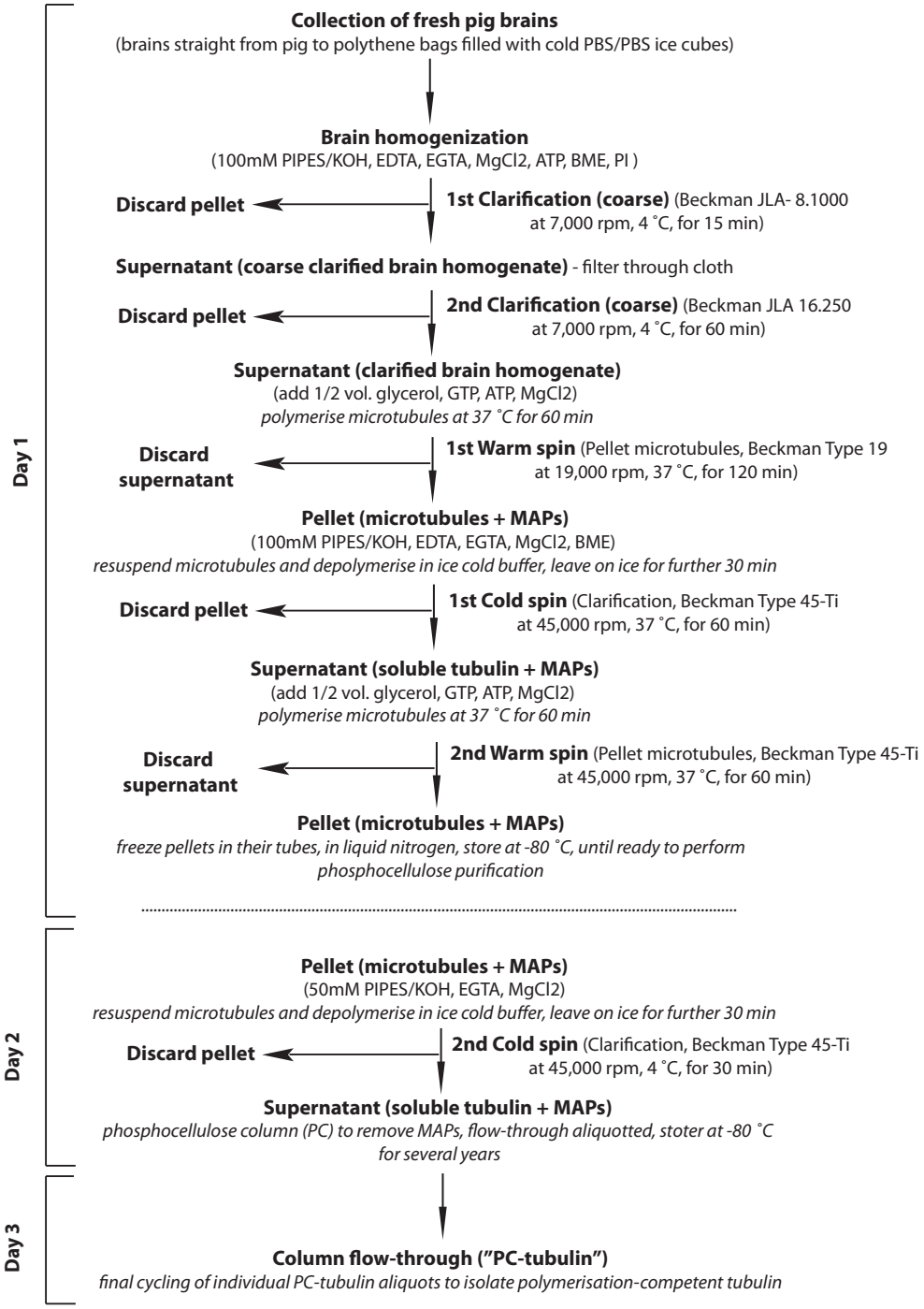

Figure 2.1: Outline of steps of purification $\alpha\beta$-tubulin from porcine brains Figure style based on [46]

ble microtubules. During the cycling process, polymerized microtubules are spun down through a glycerol cushion. The microtubules are heavy enough to pass through the cushion, but non-polymerized heterodimeric $\alpha\beta$-tubulin is not (Fig. 2.2). After the cycling, the tubulin protein is aliquoted and snap frozen in liquid nitrogen for subsequent long-term storage at -80 ℃.

The tubulin concentration is measured by a NanoDrop spectrometer. The tubulin concentration is measured at 280 nm, using a dilution series in 1x BRB80 (80 mM PIPES/KOH, 4 mM $MgCl_2$), with blank being 1x BRB80. One can calculate the final concentration from $A_{tub} = I \times C_{tub} \times \varepsilon$, where A_{tub} denotes the absorption, I the path length of the cuvette, C_{tub} the concentration in mol/L, and ε is the extinction coefficient equal to 115,000 $M^{-1}cm^{-1}$.

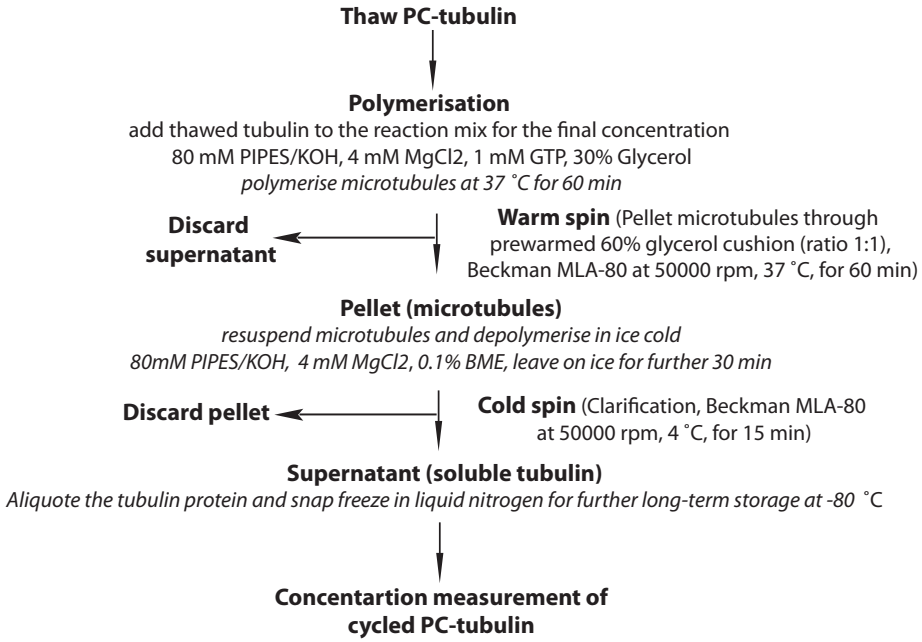

Figure 2.2: Outline of steps of PC-tubulin cycling

2.1.3 Labeling PC-Tubulin with TAMRA

The PC-tubulin is labeled with TAMRA (Invitrogen), a rhodamine fluorescent dye. This dye binds fluorophores covalently to primary amines, the N-terminus, or cysteine groups of tubulin. The protocol of tubulin labeling consists of the step of microtubule polymerization, then microtubule centrifugation through a glycerol cushion to remove all non-polymerized tubulin, followed by microtubule labeling with fluorescent dye, spinning

down the labeled microtubules though the glycerol cushion to get rid off non-reacted fluorescent dye, with subsequent microtubule depolymerization to get soluble labeled heterodimeric tubulin. The second microtubule polymerization ensures that the labeled tubulin is able to form microtubules. The final step of depolymerization results in soluble labeled tubulin, which can be snap frozen in liquid nitrogen for long-term storage at -80 ℃ (Fig. 2.3).

The quantification of the labeled tubulin concentration and labeling stoichiometry is based on the measure of both absorption of tubulin protein at 280 nm and of TAMRA at 555 nm obtained with the NanoDrop spectrometer. The concentration of tubulin in mg/mL is given by:

$$C_{tub} = \frac{A_{tub} - A_{dye} \cdot CF}{1.15},$$

where A_{tub} is the tubulin absorbance at 280 nm, A_{dye} is the dye absorbance at 555 nm, CF is a correction factor to account for dye absorbance at 280nm (for TAMRA $CF = 0.3$).
The stoichiometry of labeling is then given by:

$$D_{lab} = \frac{A_{dye} \cdot 110,000}{C_{tub} \cdot \varepsilon_{dye}},$$

where ε_{dye} is the extinction coefficient of the dye (for TAMRA $\varepsilon_{dye} = 65000$).

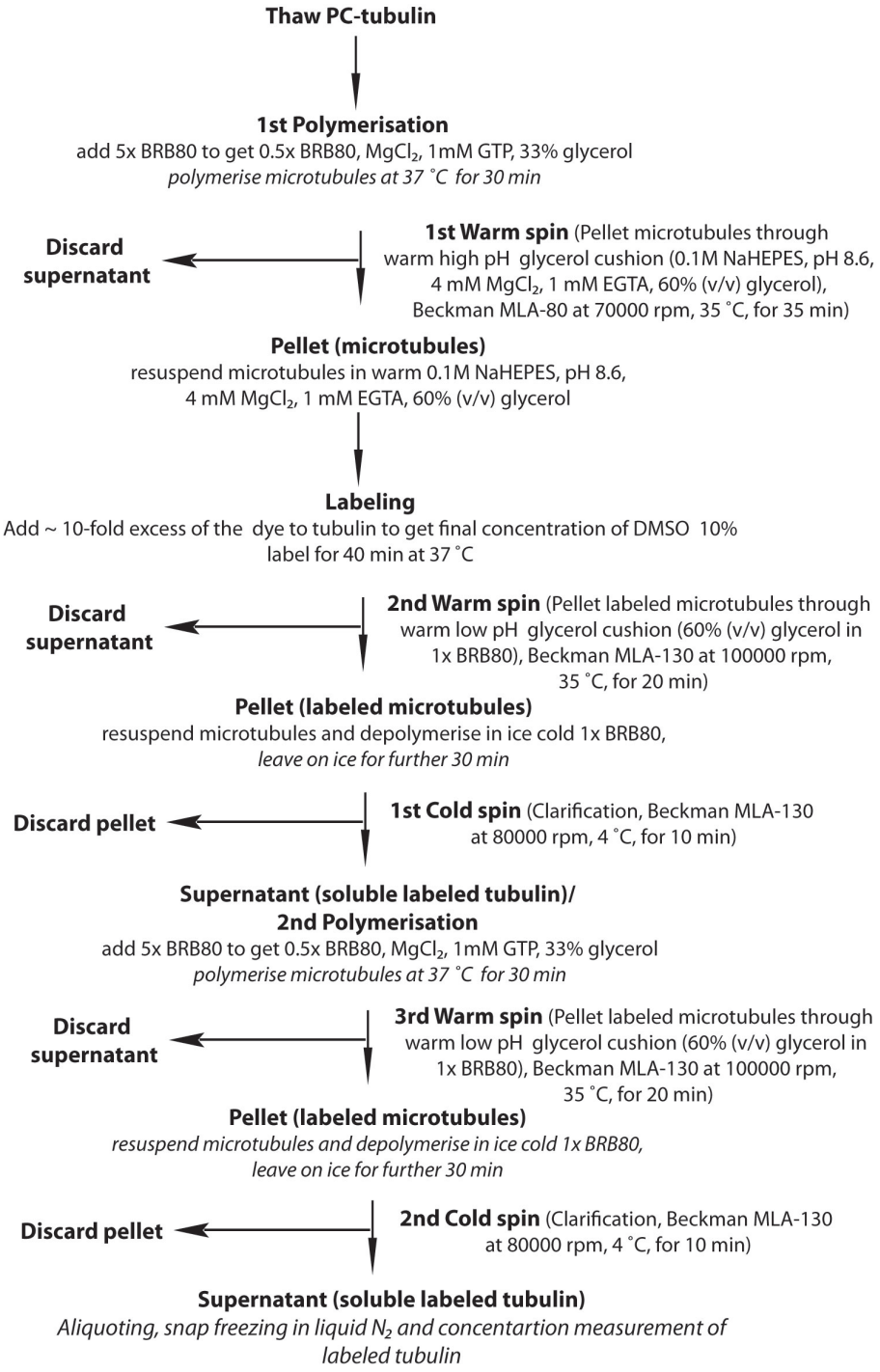

Figure 2.3: Outline of steps of PC-tubulin labeling with TAMRA

2.2 XMAP215 Expression and Purification

2.2.1 Over-expression System for XMAP215 Tagged with GFP and His7

The coding gene of XMAP215 was modified by sequential addition of a C-terminal enhanced green protein (GFP) and a C-terminal His7 tag cloned into pFastBac1 vector. Then, a baculovirus was generated from this construct for the BAC-to-BAC baculovirus expression system (Invitrogen) [22]. For this purpose, I have done a transposition of pFastBac1 into the baculovirus genome of *E.coli* strain DH10BAC.

Then the antibiotic selection of the recombinant virus bacmid shuttle vector was performed. The cells with the recombinant virus bacmid grew white in a background of blue cells. I picked up seven white colonies and one blue for the control and performed the second round of antibiotic selection (the "back-up plate"). I also checked selected colonies with PCR to verify the presence of the bacmid transposed with pFastBac1 with the inserted gene of interest. The idea of PCR screening is that the virus bacmid with pFastBac1 and the inserted gene of interest is heavier than just the bacmid alone or the bacmid with an empty pFastBac1.

After PCR screening, I picked up four colonies from the "back-up plate" and purified the bacmid DNA with the Perfectprep BAC kit 96 (5 PRIME). Then I transfected 400 µL of insect SF+ cells with 5 µL of the purified virus bacmid in the presence of Escort IV reagent and after four days harvested the passage 1 (P1) virus.

For the large-scale expression of XMAP215-GFP-His7, I prepared baculovirus infected insect cells (BIIC) stock. For that, I infected 50mL of SF+ cells with 50 µL of P1 virus and after 24 hours pelleted the cells with subsequent snap freezing for storage in liquid nitrogen. Then I performed a time-coarse of protein XMAP215-GFP-His7 full-length expression. I observed the peak of the expression after 85 hours.

Finally, for large-scale expression, 2x500 mL of SF+cells were infected with 2x100 µL of BIIC. After 85 hours the cells were pelleted, resuspended in ice-cold lysis buffer (50 mM Hepes pH 7.5, 200 mM NaCl, 5% glycerol, 0.1% Triton X-100), frozen as pearls in liquid nitrogen and stored at -80 ℃ for subsequent purification.

2.2.2 Purification of Recombinant Protein XMAP215 Tagged with GFP and His7

The purification of the recombinant protein was done in three steps. For the first step, the cation exchange column was used to get rid of all negatively charged proteins. For the second step, I used a Ni-affinity column to which the His7-tag binds strongly and all other proteins lacking the His repeats pass thought the column. Finally, for the last step, I used a size exclusion chromatography column.

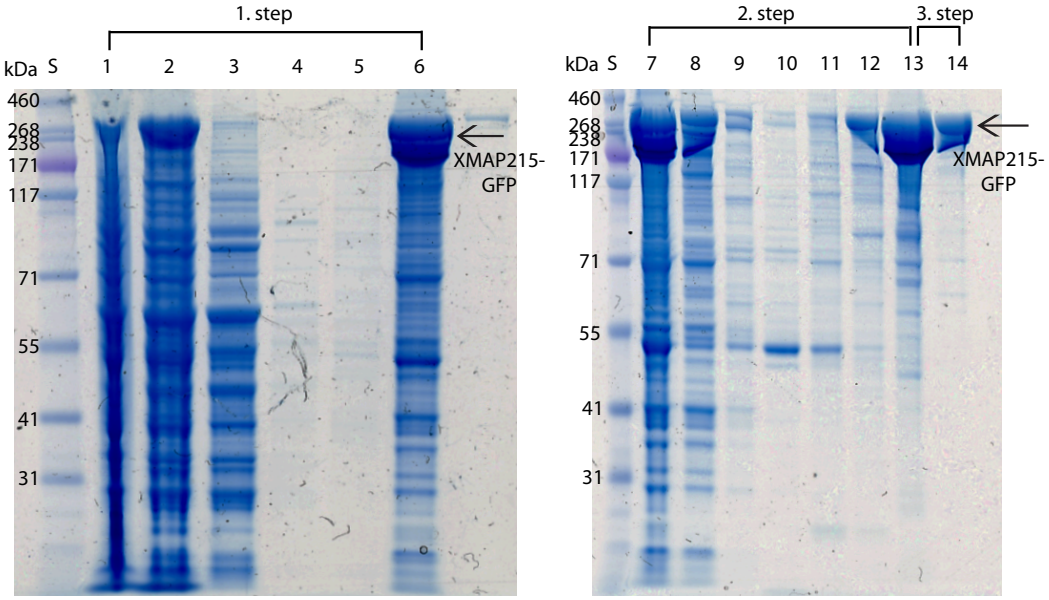

Figure 2.4: SDS-Page gels of XMAP215 purification. The XMAP215 purification is done in three steps. For the first step, the cation exchange column is used. The progression of this step can be seen in the SDS-Page gel in the following order: 1. cell lysate before centrifugation, 2. supernatant of the centrifuged cell lysate loaded onto the cation exchange column, 3. the flow through, 4. wash with 75 mM NaCl, 5. wash with 150 mM NaCl, 6. elution with 600 mM NaCl. The second step is the purification with the Ni-affinity column. The progression of this step is the following: 7. load onto the Ni-affinity column, 8. flow through, 9. wash with 9mM Imidazole, 10. wash with the high salt buffer, 11. wash with 60mM Imidazole, 12. wash with 120mM Imidazole, 13. elution of XMAP215 with 300mM Imidazole. The third step is a size exclusion chromatography column. 14. peak fractions of XMAP215 after passing through the size exclusion chromatography column. The protein standard was HiMark™ prestained (Invitrogen) (denoted as S on the gel pictures).

The frozen cells were thawed on ice. After addition of 1mM $CaCl_2$, 1x protease inhibitors mix (1 µg/mL AMPSF, 10 µg/mL antipain-HCl, 6 µg/mL chymostatin, 2 µg/mL aprotinin, 0.7 µg/mL pepstatin A, 0.5 µg/mL leupeptin and 10 µM E64) the cells were homogenized with a pre-chilled douncer. The lysed cells were centrifuged in MLA80 rotor at 80,000rpm, 4°C for 45 min. The pellet was discarded. To the supernatant I added Lysis buffer without salt (50 mM Hepes pH 7.5, 5% glycerol, 0.1% Triton X-100) to lower the NaCl concentration to 100mM. The obtained supernatant was loaded onto a SP-sepharose column (5 mL HiTrap SP HP, Pharmacia) equilibrated with cation buffer containing 75 mM NaCl (6.7 mM MES, 6.7 mM HEPES pH 7.2, 6.7 mM $C_2H_3NaO_2$, 75 mM NaCl). The column was washed with a cation buffer containing 75 mM NaCl and subsequently with one containing 150 mM NaCl. The protein was eluted from the

column with cation buffer containing 600 mM NaCl. The peak fractions were pooled, brought to 9 mM Imidazole, and loaded onto a Ni^{2+}- sepharose column (1 mL HisTrap, Pharmacia) equilibrated with a Ni-affinity buffer (25 mM Tris-HCl pH 8.0, 300 mM NaCl, 20% glycerol, 9 mM imidazole). The column was washed with 9mM imidazole, a high salt buffer (Ni-affinity buffer with 60 mg/mL NaCl), and with a Ni-affinity buffer containing 60mM Imidazole and 120mM Imidazole . XMAP215-GFP-His7 was eluted at 300mM Imidazole. The peak fractions were pooled and loaded onto a size exclusion chromatography column (GE Healthcare Superdex 200 16/60, 24 mL) pre-equilibrated with gel filtration buffer (10 mM Tris Base, 10mM Bis-Tris, 100mM KCl). The peak fractions were chosen and pooled (Fig. 2.4).

The concentration of the protein was measured with the NanoDrop spectrometer. For this purpose, the protein was degraded in 4 M urea. The Nanodrop was blanked against 4 M urea. Based on the absorption at 280nm, the concentration of the protein was calculated. The concentration of the protein in M is given by: $A = I \times c \times \varepsilon$, where A denotes the absorption, I the path length of the cuvette equal to 1 cm, c the concentration in mol/L, and ε the extinction coefficient equal to 154,900 $M^{-1}cm^{-1}$. After addition of 1mM DTT and 10% glycerol, the protein was snap frozen in liquid nitrogen and stored at -80 ℃.

Table 2.1: Buffers used for the purification of XMAP215-GFP

Buffer	**Discription**
Lysis buffer	50 mM Hepes pH 7.5, 5% glycerol, 0.1% Triton X-100, 200mM NaCl
Lysis buffer w/o NaCl	50 mM Hepes pH 7.5, 5% glycerol, 0.1% Triton X-100
Cation buffer w/o NaCl	6.7 mM MES, 6.7 mM HEPES pH 7.2, 6.7 mM $C_2H_3NaO_2$
Ni-affinity buffer w/o Imidazole	25 mM Tris-HCl pH 8.0, 300 mM NaCl, 20% glycerol
Gel filtration buffer	10 mM Tris Base, 10mM Bis-Tris, 100mM KCl

Chapter 3

Optical Tweezers

This chapter provides an explanation of the optical trapping phenomenon, a description of the apparatus, and the calibration of the optical tweezers used for my experiments. Here, I also explain the feedback technique to keep a force constant, which is essential for the applied-force experiments

3.1 Theoretical Background of Optical Trapping

In 1970 A. Ashkin et al. [11] showed that small dielectric objects can be trapped in a tightly focused laser beam. Based on this effect, an apparatus was constructed that can manipulate nanometer- and micrometer-sized dielectric particles by changing the lateral and axial position of the trapping laser focus. Because of this capability, the device was named *optical tweezers*. A micrometer-sized dielectric object can be trapped because of the interaction with the incident tightly focused laser light. This phenomenon can be explained by different theories depending on the size of the dielectric object D relative to the wavelength λ of the trapping laser. If the size of the object is much large than the laser wavelength ($D \gg \lambda$) then *geometric optics* can be used, if the size of the object is much smaller than the laser wavelength ($D \ll \lambda$) then the *Rayleigh theory* is valid, and if the size of the object is comparable with the laser wavelength ($D \approx \lambda/2\pi$) then the exact electromagnetic theory is needed.

Geometric optics. According to *geometric optics*, light can be represented as a bundle of the rays. Each ray has a momentum proportional to its intensity. When a light ray encounters a dielectric object (from now onwards referred to as a polystyrene microsphere or bead), it is reflected and refracted at the interface between the object and the medium according to *Snell's law*: $n_m \sin\theta_i = n_o \sin\theta_r$, where n_m is the refractive index of the medium, n_o the refractive index of the object, θ_i the incident angle of the light ray, and θ_r the refractive angle. If the refractive indexes of the medium and the microsphere differ, then the light ray will deviate from the initial path causing a change in its momentum. Because of momentum conservation, the microsphere experiences an equal and opposite momentum change. The net momentum change of all rays in the light beam gives a rise

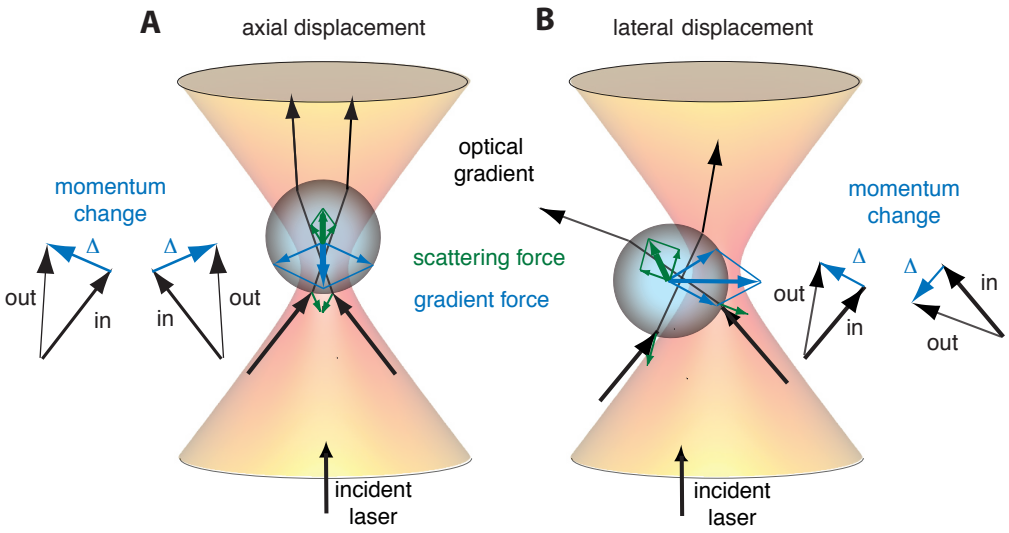

Figure 3.1: Geometric optics description of the scattering and gradient forces. A polystyrene bead is trapped in the tightly focused laser beam. The incident laser light is represented by two rays (black lines with different thickness representing the light intensity). The incoming rays are refracted two times passing through the bead, and, therefore, their momentum is changed. This is illustrated by the difference Δ of the momentum of the entering (in) and leaving ray (out) at the vector diagrams (**A**) and (**B**). Because of momentum conservation, the bead will experience an equal and opposite momentum change, which results in *the gradient force* shown as a blue arrow. In (**A**), the bead is displaced above the laser focus. The moment change leads to the gradient force pointing down towards the focus and resulting in axial movement of the bead into the laser focus. In (**B**), the bead is displaced to the left from the focus. The momentum change leads to the gradient force pointing to the right, and, thereby, displacing the bead laterally into the laser focus. The incident light is also reflected by the bead (depicted by green arrows). This leads to *the scattering force* that acts in the propagation of the direction and, hence, tends to destabilize the optical trap.

to a *gradient force* pushing the object towards the region of highest light intensity. On the other hand, some of the light rays are reflected by the microsphere. When a light ray is reflected, it changes the direction of the initial path and hence its momentum is changed as well. Therefore, the equal and opposite momentum change is transferred to the microsphere. The net momentum change of the reflected rays give rise to a *scattering force* pushing the bead out of the region of highest light intensity. As a result, these two forces compete with each other. And the dielectric object can be trapped if the *gradient force* is higher than the *scattering force* (Fig. 3.1) [12].

Rayleigh approximation Electromagnetic fields induce a polarization of dielectric objects. If the microsphere is much smaller than the wavelength of the trapping laser then it can be treated as a point dipole. In an electromagnetic field with an intensity

gradient, the point dipole experiences a force that can be decomposed into two forces: a *gradient force* and a *scattering force*. The *gradient force* results from the Lorentz force acting on an induced dipole in an electromagnetic field with an intensity gradient. It scales with $F_{grad} \propto R^3 \nabla E^2$, where E is the magnitude of electric field and R is the radius of a microsphere. This force brings the microsphere towards the region of highest intensity of the electromagnetic field. The *scattering force* is due to the scattering of an electromagnetic wave by a point dipole. This force scales with $F_{scat} \propto R^6 E^2$ [51].

Electromagnetic theory If the size of a microsphere is comparable with the wavelength of the trapping laser then it is necessary to use the exact electromagnetic theory to explain the phenomenon of trapping. In this case, it is treated as a scattering problem. The analytical solution for the scattering of a light *plane wave* by a sphere is provided by the Lorenz-Mie theory. However, the laser light in optical tweezers is not a *plane wave*, but a tightly focused beam. This causes certain difficulties for the mathematical description of it. Nevertheless, forces can be calculated numerically [92].

3.2 Optical trap: a Hookean spring in three dimensions

The microsphere trapped in a tightly focused laser beam is located in a three-dimensional potential well. For small displacements of the bead, the potentials are quadratic, for the x-direction, e.g. given by:

$$U = \frac{\kappa x^2}{2}.$$

The force keeping the microsphere in the potential results from:

$$-\frac{dU}{dx} = F = -\kappa x.$$

Hence, if the bead is displaced from the laser focal spot, a restoring force brings the bead back to the focus. The magnitude of the restoring force is proportional to the displacement from the focal spot. This is nothing else, but *Hooke's law*. Therefore, the optical trap can be represented as a Hookean spring in three dimensions.

3.3 Optical tweezers is a tool to apply piconewton forces and detect nanometer displacement

Optical traps are very sensitive instruments and are able to detect a sub-nanometer displacement of a sub-micrometer dielectric particle, usually a polystyrene microsphere, with high temporal resolution. Because of this optical tweezers are widely used in biology to measure the interaction of e.g. kinesin proteins, DNA machinery proteins, kinetochore proteins, microtubule associated proteins with their respective substrates.

3.4 Optical tweezers setup used for the DIC imaging and the experiment with stationary optical trap

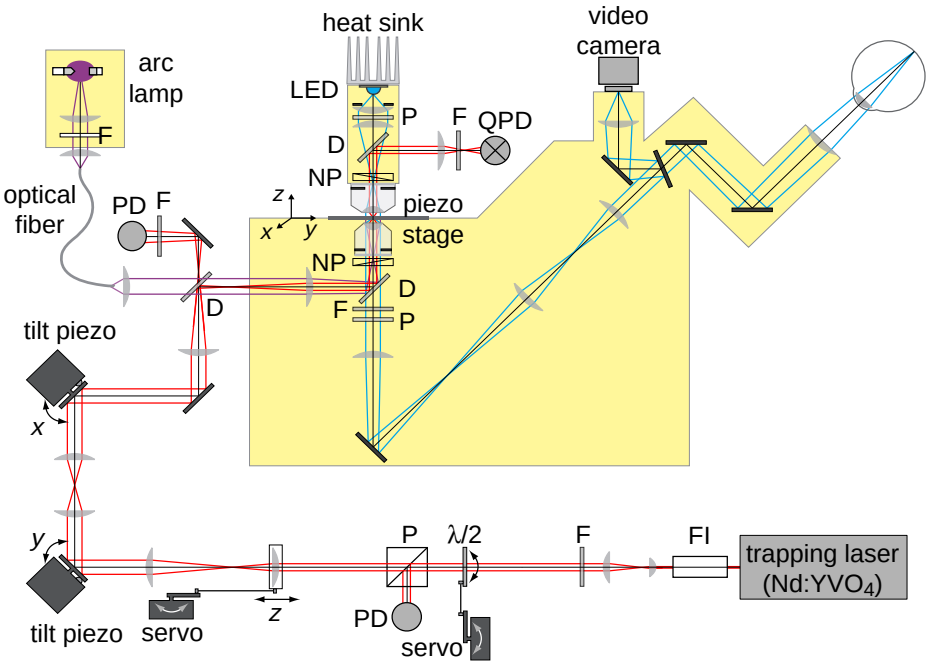

Figure 3.2: Schematic drawing of the optical tweezers setup. All the optical components are shown. The trapping laser path is depicted in red and the image path is blue. The labeled components of optical tweezers are: Faraday isolator (FI), filter (F), half-wave plate ($\lambda/2$), polarizer (P), photo-diode (PD), dichroic mirror (D), Nomarski prism (NP), light emitting diode (LED), quadrant photo- diode (QPD). (Adopted from [103])

The optical tweezers setup was built around an inverted microscope (Zeiss Axiovert 135 TV) on an optical table. The schematic drawing with all elements and the light path is shown in Fig. 3.2. For a detailed description see [103], [18].

3.5 Optical tweezers setup used for the experiment with a force feedback

For constant force measurements another setup was used, which is described in detail in [77]. The setup is schematically depicted in Fig. 3.3.

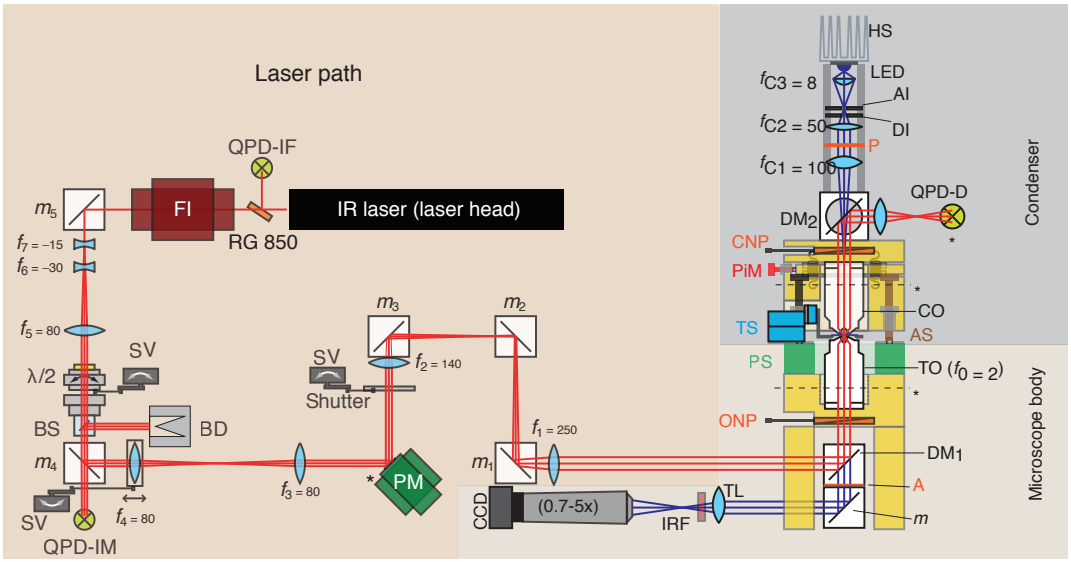

Figure 3.3: The schematic drawing of optical tweezers setup. All the optical components are shown. The trapping laser path is depicted in red and the image path is in blue. The labeled components of optical tweezers are: quadrant photo- diode for intensity feedback (QPD-IF), Faraday isolator (FI), laser mirrors (m_{1-5}), lenses ($f_1 - 7$), half-wave plate ($\lambda/2$), servo(SV), beam splitter (BS), beam dump (BD), quadrant photo-diode for intensity monitoring (QPD-IM), piezo mirror (PM), piezo translation stage (PS), S, stage; PSD, position sensitive diode. All focal length are in mm. The parts of a home-built microscope: heat sink (HS), light emitting diode (LED), lens (f_{c1-3}), aperture iris (AI), field diagram iris (DI), polarizer (P), condenser Nomarski prism (CNP), quadrant photo- diode for detection (QPD-D), dichroic mirror (DM_{1-2}), condenser objective (CO), pico motor (PiM), traveling stage (TS), adjustment screw (AS), piezo stage (PS), trapping objective (TO), objective Nomarski prism (ONP), analyzer (A), mirror (m), tube lens (TL), infrared blocking filter (IRF), charge-coupled device (CCD).The dashed lines across the trapping and condenser objectives indicate the back focal plane. The asterisks indicate conjugate planes. (Adopted from [76])

3.6 Calibration of Optical Tweezers

In the optical trap, the microsphere is held by the trapping force. This force balances the thermal force, causing Brownian motion, damped by the drag force due to the viscosity of the medium. Since the trapping force can be described by *Hooke's law*: $F_{trap} = \kappa \cdot \Delta x$, one can measure the trapping force if the trap stiffness κ and the microsphere displacement from the laser focus Δx are known. The lateral and axial position of the microsphere are monitored by a quadrant photo diode (QPD). The read out from the QPD is in volts. To get the position of the trapped microsphere in nanometers one needs to calculate the conversion factor β in nm/V, also called sensitivity factor, or, in other words, calibrate the detection system. The trap stiffness κ can be calculated from

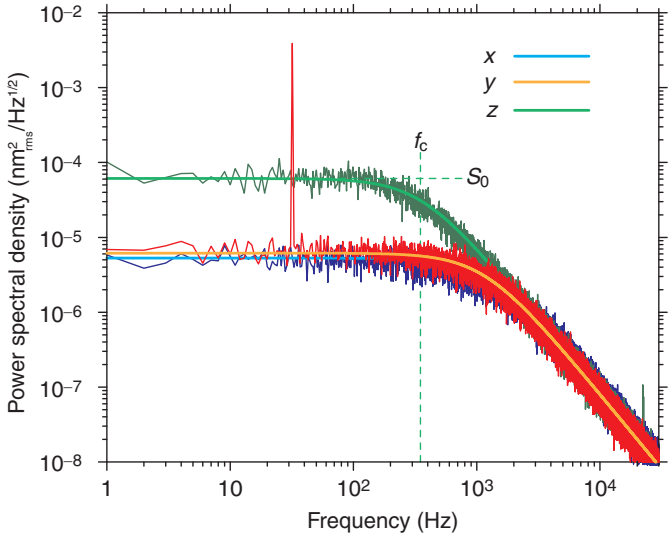

Figure 3.4: Optical trap calibration. Example of a calibrated power spectral density of a trapped 0.528 µm microsphere for x-, y-, and z-directions. The calibration spike on the y-direction at $f_{stage} = 32$ Hz results from oscillating the stage at the same frequency. Each power spectrum is an average of 40 independent spectra. The vertical dashed line indicates the corner frequency $f_c$and the horizontal dashed line indicates the plateau S_0 for the axial direction. The sampling rate was 102400 Hz at a resolution of 1 Hz. Each spectrum is fitted with a Lorentzian (bright line). (Taken from [76])

the forces acting on the trapped microsphere.

In our setup we use the calibration method described in [115], in which the displacement of a trapped bead is measured in response to a known flow. In this method, the sample is moved by a piezo-stage sinusoidally with known amplitude (0.5 - 1 µm) and frequency (32 Hz) relative to the optical trap. In a power spectrum, this motion results in a Lorentzian-type power spectrum, characterized by a plateau value S_0 and corner frequency f_c, with an additional spike at the oscillation frequency (32 Hz). The height of this spike serves as a scale bar for the sensitivity factor β:

$$\beta = A\sqrt{2P_{spike}\Delta f(1 + \frac{f_c^2}{f_{oscil}^2})},$$

where A is the amplitude of the oscillations, $P_{spike}\Delta f$ is the measured power in the spike, f_c is a corner frequency of the Lorentzian-type power spectrum and f_{oscil} is the frequency of the oscillations.

Knowing the displacement sensitivity β, one can calculate the trap stiffness κ using $f_c = \frac{\kappa}{2\pi\gamma}$, where γ is the drag coefficient, and the Einstein-Smoluchowski equation

$D = \frac{k_b T}{\gamma}$, where the diffusion coefficient in nm^2/V is equal to $D = \beta^2 \cdot 2\pi^2 S_0 f_c^2$. The trap stiffness is given by:

$$\kappa = \frac{k_b T}{\pi \beta^2 S_0 f_c}.$$

3.7 Force feedback

In a dynamic microtubule assay, a microsphere, covered with XMAP216-GFP-His7, is positioned at the growing microtubule tip by the optical trap. If the optical trap is stationary then the microsphere following the microtubule growth will move away from the laser focus after some time. This will give rise to a restoring force proportional to the microsphere displacement from the laser focus. At a certain displacement, the force will become large enough to detach the microsphere from the microtubule tip and bring it back to the optical trap center. On the other hand, if the optical trap can follow the bead movement with a fixed offset between the center of the microsphere and the laser focus then a constant trapping force will act on the microsphere. If the offset is equal to zero then the trapping force is equal to zero and one can follow the movement of the microsphere with optical trap without any force applied. However, in practice it is not possible to keep the offset equal to zero, therefore a certain small offset is kept to give rise to a small constant trapping force ($\sim$ 0.1 pN). By increasing the offset between the microsphere center and the laser focus, one can set the desired constant force acting on it. Depending on where the optical trap is with respect to the bead center the applied force can be pushing or pulling. To follow the position of the microsphere with the constant force a feedback is required, which will maintain the same offset between the bead center and the optical trap canter over time. In our setup, we used a feedback based on a proportional-integral-derivative (PID) controller.

3.7.1 PID controller method.

To maintain the same offset between the laser focus and the center of the bead, the feedback loop needs to read a process variable, the actual position of the bead with respect to the optical trap position, calculate the difference between it and a set point, the desired offset, and give an output to compensate for any error. The error is the difference between the desired offset and actual position. The output signal according to the PID controller method can be represented as a sum of *proportional, integral* and *derivative* terms:

$$U(t) = Pe(t) + I \int_0^t e(\tau)\, d\tau + D \frac{de(t)}{dt},$$

where P is the proportional gain, I the integral gain, D the derivative gain, e the error and t time [60], [13].

The *proportional gain* P makes the feedback output proportional to the error magnitude e. Used alone, the *proportional gain* gives rise to a finite difference between set point and a process variable, a so-called steady-state error. The *integral gain* I sums

the error term over time and, hence, proportional to both the error magnitude e and the duration of the error τ. This term accelerates the process of reaching the desired set point and removes the residual steady-state error from the feedback output signal, although it may give rise to the so-called overshoot error, when the output feedback signal overshoots the set point. To eliminate the overshooting problem, the *derivative gain* D is used. It is proportional to the rate of change of the process variable. One needs to use it carefully because, in very noisy systems, this term can add noise or destabilize the feedback.

3.7.2 Tuning the feedback parameters.

In our setup, a two-dimensional PID feedback is implemented in Labview. The feedback calculates the proportional, integral and derivative gains separately. The laser focus is moved by a piezo tilt mirror in the x- and y- directions according to the output signal of the feedback. Therefore, the QPD signal of the bead position remains close to constant and the main information about the trapped microsphere position is contained in the mirror sensor signal: $x_{bead} = -(x_{mirror} + x_{QPD})$. During the measurements, we acquired eight signals: three signals from the QPD of the x, y and z position of the trapped microsphere, the three monitor signals x, y and z of the piezo stage and two signals x and y of the piezo tilt mirror.

In my experiment, I want to follow XMAP215 attached to the microsphere surfing a dynamic microtubule end. Is microtubule growing stepwise by the addition of the 8 nm tubulin dimers? To answer this question, my ultimate goal is to resolve 8 nm steps. To tune the feedback parameters, I used the so-called trial and error method. According to it, the P value needs to be increased until oscillations occur and then decreased again for a suitable fast response. Then, the I parameter is optimized to minimize the steady-state error and avoid overshoot. Finally, the D parameter is increased until the loop is quick to reach the set point.

First, I immobilized carboxyl-modified polystyrene microspheres of 0.59 µm in diameter on the glass surface of my flow cell. Then I simulated 8 nm steps with a frequency of 3 Hz by a random stepwise movement of the piezo stage. To tune the feedback parameters, I followed this simulated movement with the mirror feedback until the 8 nm steps were clearly resolved. The feedback rate, how many times per second the feedback updates the microsphere position, was chosen to be 1000 Hz. The feedback rate has to be lower than the corner frequency f_c of the power spectrum of the trapped microsphere to avoid amplification of the Brownian motion.

Then, to make the situation resemble to my experimental conditions, I attached an antibody specific to the C-terminus of XMAP215 to the glass surface of the flow cell and blocked the remaining surface with Pluronic F-127 to prevent non-specific interactions. When the XMAP215-GFP-His7-coated microsphere was brought into contact with the flow cell surface, the antibody reacted with XMAP215 and the microsphere became at-

tached. Then, I simulated the 8 nm steps with the piezo stage and followed the position of the attached microsphere with the mirror feedback. Because of the long PEG linker (see below), I could not resolve 8 nm steps. However, 20 nm steps at 3 Hz were clearly resolved with fine-tuned PID parameters and 1000Hz feedback rate.

Chapter 4

Experimental setup and conditions

To study the addition of tubulin dimers at the microtubule end by XMAP215 with and without applied external force, I reconstitute in vitro the interaction of dynamic microtubule ends with XMAP215 molecules coupled to a polystyrene microsphere. This coupling is essential for both the position detection of the microsphere reflecting the position of XMAP215 molecules attached to it and the force application. In the following chapter, I describe both the protocol of coupling XMAP215 molecules to the surface of a polystyrene microsphere and the in vitro assay for reconstitution of the interaction of dynamic microtubule ends with XMAP215 molecules.

4.1 Coupling XMAP215-GFP-His7 to Polystyrene Microspheres

To perform optical tweezers experiments, I need to use a polystyrene microsphere as a handle to manipulate XMAP215-GFP-His7. In my assay, the protein XMAP215-GFP-His7 is immobilized on the surface of a polystyrene microsphere through a linker consisting of polyethylene glycol molecule (PEG) and an antibody specific to GFP. The PEG is covalently attached to the microsphere surface and the antibody is covalently attached to the PEG molecule. Then, XMAP215-GFP-His7 is incubated with the modified polystyrene microspheres. The antibodies bind to the GFP-tag anchoring the protein to the surface of the bead.

4.1.1 Covalent Binding of PEG Molecules and GFP Antibodies to the Surface of a Polystyrene Microsphere

PEG molecules are bound to a polystyrene microsphere via a covalent interaction between COOH- groups of carboxyl-modified polystyrene microspheres and NH_2 of amino-modified PEG molecules. In my assay, there are two types of the PEG molecules coupled to the microsphere surface. One type has a molecular weight of 2 kDa, which has at

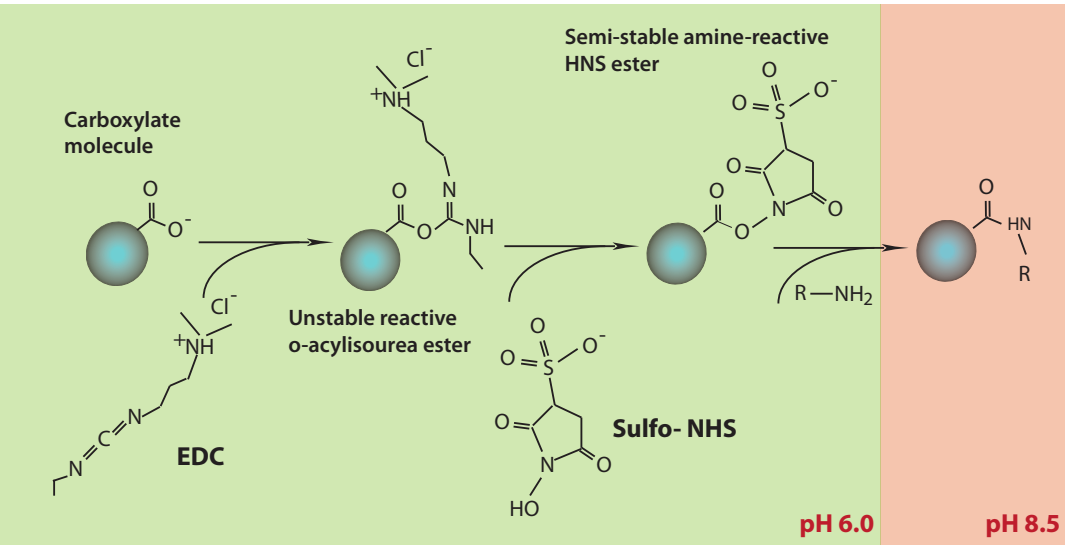

Figure 4.1: Covalent coupling of PEG molecules containing amino groups to the carboxylated microspheres. Two-step procedure for coupling amino containing molecules to carboxylated beads. In the first step at pH 6.0, the carboxylated groups on the beads are activated using EDC. The resulting short-lived ester reacts with sulfo-NHS forming a more stable amine-reactive intermediate. Before adding the target molecules, the pH is raised to 8.5, promoting the covalent attachment of the amine groups to the sulfo-NHS ester via peptide bonds during the second reaction step. Adapted from [53]

one end of the chain an amino group (-NH_2) and at the other end a methoxyl group (-CH_3O) (Table 4.2). The second type is a 3 kDa PEG molecule, which also have at one end of the chain an amino group (-NH_2) and at the other end carboxyl group (-COOH) (Table 4.2). These two types of molecules are mixed in a 9:1 ratio, respectively. Such a mixture ensures the hydrophilic properties of the microspheres because of the 2 kDa PEG molecules with free methyl groups. As a consequence, the modified particles do not aggregate. On the other hand, the mixture gives the possibility to couple covalently a GFP antibody via carboxyl groups of the 3 kDa PEG molecules and the amino groups of the antibodies.

Covalent binding of PEG molecules to the polystyrene microsphere. The first step of the protocol is to couple the PEG molecules. To do this, 25 µL carboxyl-modified microspheres (Table 4.1) were pelleted 2 times in 1000 µL of 50 mM MES pH 6.0 at 13,000 g for 3 min and resuspended in 250 µL of 50mM MES pH 6.0. To activate the COOH-groups on the microspheres, 1.62 mg of N-hydroxysulfosuccinimide sodium salt (sulfo-NHS, Table 4.2) and 1.42 mg of N-(3-dimethylaminopropyl)-N′-ethylcarbodiimide hydrochloride (EDC, Table 4.2) were added sequentially (Fig. 4.1). The particles were incubated in a thermoshaker at 600 rpm, at 37 ℃ for 15 min. After the incubation the

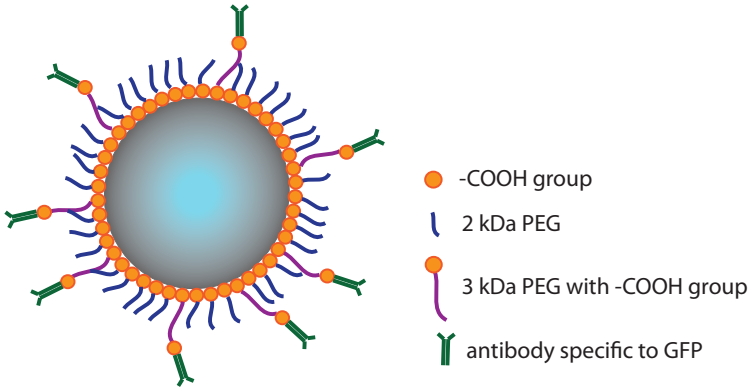

Figure 4.2: Covalent coupling of antibodies specific to GFP via PEG linker to the surface of carboxylated polystyrene microsphere. Two types of PEG molecules are covalently coupled through their amino groups to the carboxyl groups of the polystyrene bead. One type of PEG molecules is shorter with a molecular weight of 2 kDa and the other is longer with a molecular weight of 3 kDa. The 3kDa PEG molecules have the carboxyl group at the free end to which the GFP antibodies are covalently coupled via their amino groups. (The figure is not drawn to scale)

microspheres were washed 2 times in 500 µL 50 mM MES pH 6.0 to get rid of non-reacted sulfo-NHS and EDC. The beads were resuspended in the PEG solution (9.36 mg of 2 kDa NH_2-PEG-CH_3O and 1.56 mg of 3 kDa NH_2-PEG-COOH in borate buffer pH 8.5) with an incubation in the thermoshaker at 600 rpm, at 37 ℃ for 2 hours. After the incubation time, the particles were washed 5 times in 500 µL of borate buffer pH 8.5, 3 times in 500 µL of 50 mM MES pH 6.0 and resuspended in 250 µL of 50 mM MES pH 6.0 for the subsequent second step of covalent coupling of antibodies specific to GFP.

Table 4.1: Properties of polystyrene microspheres used for XMAP215-GFP coupling

Property	**Value**
Mean diameter (µm)	0.59
Polymer description	P(S/V-COOH)
Density (g/cm^3)	1.06
Surface groups	COOH/1
Surface charge (µeq/g)	28.5
Parking area (sq.A/grp)	56.4
% Solids (w/w)	10
Product number	PC03N/6487
Company	Bangs Laboratories

Covalent binding of a GFP antibody to the PEG molecules. During the second step of the coupling protocol 250 µL PEG-coated microspheres in 50 mM MES pH 6.0 were activated a second time by the addition of 1.62 mg of sulfo-NHS and 1.42 mg of EDC and incubation in the thermoshaker at 600rpm, at 37 ℃ for 15 min. After the activation the microspheres were washed 2 time in 500 µL of 50 mM MES pH 6.0, resuspended in 250 µL of antibody solution (45 µg monoclonal mouse antibody specific to GFP in 1x PBS) and incubated in the thermoshaker at 600 rpm, at 37 ℃ for 1 hour and then at 600rpm, at 4 ℃ overnight. Then the microspheres were washed 5 times in 1x PBS and stored at 4 ℃ before the XMAP215-GFP-His7 coupling step (Fig. 4.2).

Coupling of XMAP215-GFP-His7 to the Modified Polystyrene Microspheres. The third step of the coupling protocol is to immobilize XMAP215-GFP-His7 molecules on a polystyrene microsphere via the GFP-tag. For that purpose 47 µg of the modified polystyrene microspheres were incubated with an XMAP215 solution (96 nM XMAP215-GFp-His7, 10 mM Tris Base, 10mM Bis-Tris, 100mM KCl, 1 mM DTT) in the thermoshaker at 600 rpm, at 4 ℃ overnight. XMAP215-GFP-His 7 was freshly purified and not exposed to the freezing procedure in liquid nitrogen. Then, after addition of 10% glycerol, the XMAP215-GFP-His7 coupled microspheres were aliquoted, snap frozen in liquid nitrogen and stored at -80 ℃.

Table 4.2: Chemicals used for the covalent coupling

Name	**Chemical formula**	**MW**	**cat.#, Producer**
α-Methoxy-ω-amino PEG	CH_3O-PEG-NH_2	2 kDa	12 2000-2, Rapp Polymere GmbH
α-Amino-ω-carboxy PEG hydrochloride	H_2N-PEG-O-C_3H_6-COOH · HCl	3 kDa	13 3000-20-32, Rapp Polymere GmbH
N-(3-Dimethylaminopropyl)-N′-ethylcarbodiimide hydrochloride (EDC)	$C_8H_{17}N_3$ · HCl	191.7 g/M	130672 - 98%, Sigma-Aldrich
N-Hydroxysulfosuccinimide sodium salt (sulfo- NHS)	$C_4H_4NNaO_6S$	217.13 g/M	56485 - 98.5% (HPLC), Sigma-Aldrich

Table 4.3: Buffers used for the covalent coupling of PEG molecules and antibodies to the bead surface

Buffer	Description
MES	50mM MES (MW 195.2) pH 6.0
Borate buffer	50mM Boric acid (MW 61.83) mixed with 18mM Sodium tetraborate decahydrate (MW 381.37) to get pH 8.7
PBS	137 mM NaCl, 2.7mM KCl, 10mM Na_2HPO_4, 2mM KH_2PO_4, pH 7.4

4.1.2 Concentration Measurements of the XMAP215-coated Microspheres

The concentration of the XMAP215-coated microspheres was calculated based on the absorption values at 400 nm, 500 nm, 600 nm, 700 nm measured with a spectrometer (Agilent Technologies; Part-No. 5063-6565; Ultra-micro quartz cell 10mm, 5 µL). For this measurements several dilution series of the carboxyl-modified particles (Table 4.1) were performed, with the dilution factor of 1000, 1250, 1500, 1750, 2000, 2250, 2500, 2750, 3000, 3250, 3500, 3750, 4000, 4500. Then the prepared XMAP215-coated microspheres were diluted to a theoretical value of a dilution factor of 1000x from initial stock solution (10% solids) and the absorption of them at 400 nm, 500 nm, 600 nm, 700 nm was measured. The real dilution factor was assumed to be the same as the dilution factor of the closest absorption spectrum of the diluted carboxyl-modified microspheres. In my assay, the XMAP215-coated particles had the dilution factor of 1000 from the original stock of carboxyl-modified microspheres (10% solids) what gives the concentration of 0.1 mg/mL. Based on the concentration estimation of the microspheres and the XMAP215-GFP-His7 concentration, the ratio of the XMAP215 molecules per particle was $\sim$ 520000 molecules per a microsphere.

4.2 *In vitro* reconstitution of the interaction of dynamic microtubules with XMAP215 molecules

4.2.1 Treatment of the Cover-glasses

The goal is to produce clean cover-glasses to form a simple flow cell that allows to attach microtubule "seeds". In addition, the surface should be effectively passivated to prevent unwanted, non-specific interaction of XMAP215-coated microspheres and tubulin with the glass surface.

Two types of cover-glasses, one 18 $\times$ 18 mm^2 (Menzel, #0) and the other 22 $\times$ 22 mm^2 (Corning, #1.5), were subjected to a silanization process. This process is consist-

ing of washing the cover-glasses first with acetone for 55 min and then with absolute ethanol for 10 min in an ultrasonic bath, then cleaning with "Piranha solution" (mix of H_2O_2 and H_2SO_4 in the ratio of 1:2) for 60 min at 55 ℃ to remove all organic contaminations. After that, the cover-glasses are immersed into 0.1 M KOH for 15 min to activate -OH groups on the glass surface for silanization. Then, finally, the surface was functionalized with a hydrophobic silane that allows efficient surface passivation. The silanization was performed by immersing the cover-glasses in a 0.05% solution of DDS (dimethyldichlorosilane) in TCE (trichloroethylene) for 60 min followed by three steps of washing with methanol for 5 min, 15 min and 30 min. After the last step of washing the cover-glasses are dried with a nitrogen gun and stored in a clean, sealed glass container.

4.2.2 Chamber Preparation

To form a chamber, the two different-sized cover-glasses were used. The channels were form by cutting out two stripes in a piece of Parafilm. The Parafilm with the two formed channels was placed on the bigger silanized cover-glass and covered by the smaller one. To fix the cover-glasses together with the Parafilm, a hot stamp (130 ℃) was placed on top of the smaller cover-glass for a few seconds. Then the excess of Parafilm was cut off with a scalpel (Fig. 4.3).

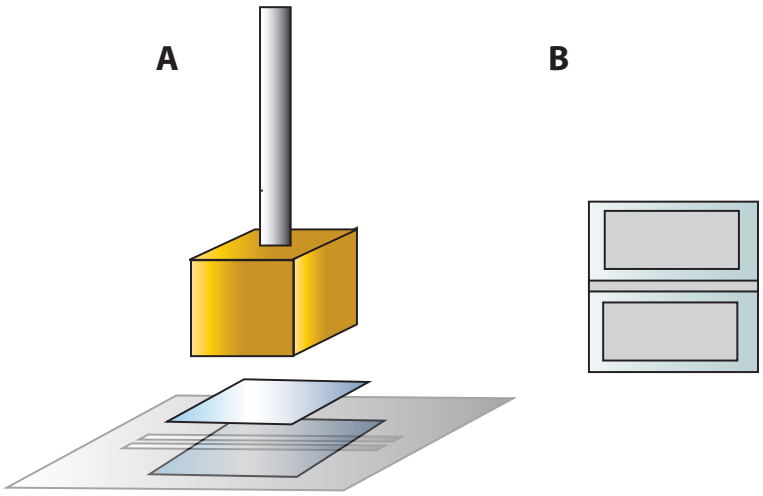

Figure 4.3: Flow cell. A. Flow cell preparation. Between two cover-glasses of different size the Parafilm is inserted. To form a channel, two stripes of the Parafilm are cut out. The cover-glasses are fixed together by melting the Parafilm **B.** Topside view of a prepared flow cell

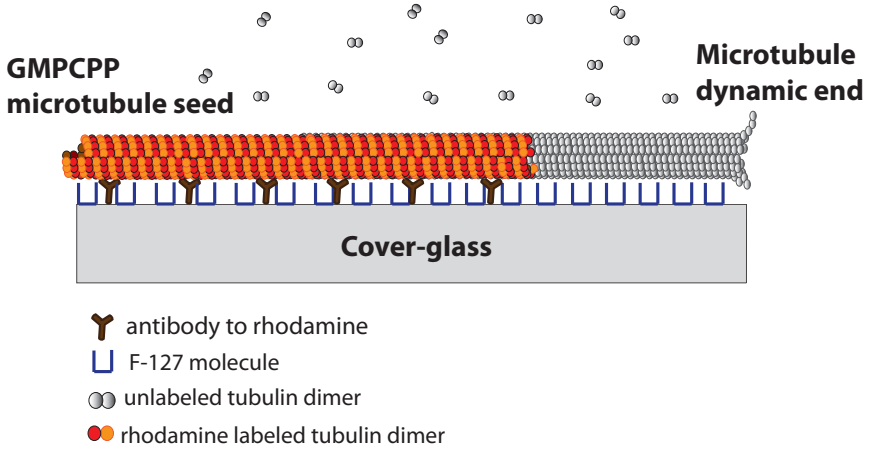

Figure 4.4: Microtubule dynamic assay. The TAMRA labeled microtubule "seeds" stabilized with GMPCPP are attached to the cover-glass surface via antibodies specific to the TAMRA dye. To prevent non-specific interactions between proteins and the glass surface, the channels were passivated with Pluronic F-127 molecules. Upon addition of the unlabeled, soluble tubulin, the microtubules start to grow and shrink from their ends, exhibiting dynamic instability.

4.2.3 Growing GMPCPP Stabilized Rhodamine labeled Microtubules

To reconstitute dynamic microtubules *in vitro*, the microtubule dynamic extensions were grown from stable seeds, which are short microtubules polymerized from 2 µM rhodamine labeled tubulin in 1xBRB80 with 1mM $MgCl_2$, and in presence of 1mM GMPCPP, a slowly hydrolyzable analogue of GTP, for 2 hours at 37 ℃. The polymerized microtubules were spun down in Beckman airfuge at 30 psi for 5 min, the supernatant was discarded, and the pellet was resuspended in 1x BRB80 to get rid off non-polymerized tubulin. To get microtubules of consistent lengths ($\sim$ 2 µm), they were sheared with a 27 gauge needle by passing them up and down three times.

4.2.4 Dynamic Microtubule Assay

After the chamber preparation, the following sequence of solutions was flowed through the channels.

First, 20 µL of 25 times diluted, rhodamine specific antibody in 1x BRB80 were passed through the channels with the help of vacuum, because of the high hydrophobicity of the glass surface, and incubated for 10 min. These antibodies allow to attach specifically TAMRA-labeled microtubule seeds. They also prevent the surface interaction between the glass and the microtubules, which facilitates the interaction between XMAP215 molecules and the microtubule lattice. Then, the channels were washed with 20 µL of 1x BRB80.

Second, 20 µL of a solution of 1% Pluronic F-127 (Invitrogen) in 1x BRB80 was flowed through and incubated for 30 min. Pluronic F-127 is a tri-block copolymer consisting of two outer poly(ethylene oxide) (PEO), also known as poly(ethylene glycol), and an inner poly(propylene oxide) (PPO) blocks with 100 and 65 monomers, respectively. The PPO block is hydrophobic and strongly adsorbs onto the hydrophobic-rendered glass surface. The outer PEO parts form a polymer brush with an approximately 10-nm thickness that is very effective in blocking protein adsorption in single-molecule experiments. Then the channels were thoroughly washed with 100 µL of 1x BRB80.

Third, 20 µL of the GMPCPP-stabilized microtubule seeds were introduced into the channel and washed with 100 µL of 1x BRB80 to get rid off all non-bound microtubules. To reconstitute *in vitro* dynamic microtubules and study the interaction between XMAP215 molecules and dynamic microtubule plus ends, the $\alpha\beta$-tubulin extensions were grown from GMPCPP-stabilized, TAMRA-labeled microtubule seeds. To do so, 20 µL of the tubulin solution together with XMAP215-coated microspheres were introduced into the channel (1x BRB80, 7.5 µM tubulin, 15 µM tubulin, 42.5 µM D-glucose, 42.5 µg/ml glucose oxidize, 17 µg/ml catalase, 10.6 mM DDT, 85 µg/ml casein, 1.25 mM GTP, 75 mM KCl, 80 times diluted XMAP215- coated microspheres) (Fig. 4.4).

Chapter 5

Results

5.1 XMAP215 harnesses microtubule growth and shrinkage energy to move a cargo

In my experiment rhodamine labeled microtubule "seeds" were attached to a coverglass surface via antibodies specific to a rhodamine dye. Upon addition of the solution with non-labeled tubulin protein and XMAP215 coated microspheres, the microtubule "seeds" started to grow dynamic extensions undergoing periods of assembly alternating with periods of disassembly. At the used tubulin concentration, the microtubules grew only from their plus-end. When the microtubule underwent a shrinkage phase, it was disassembling all the way to the stable "seed". The experiment was visualized by differential interference contrast microscopy (DIC) implemented in our optical tweezers setup [18]. The microtubule plus-end could be recognized in DIC movies as a jiggling microtubule extension. It is driven by collisions with the surrounding particles undergoing Brownian motion. The dynamic microtubule plus-end was jostling because it did not interact with the surface as it consisted of only unlabeled tubulin protein.

The XMAP215-coated microspheres were tested for microtubule binding with the help of an optical trap. Each candidate bead was trapped and brought to the vicinity of the microtubule growing end and positioned on it. After slightly pressing the bead against the microtubule plus-end for approximately one minute, the optical trap was switched off, and the XMAP215 coated bead remained attached to the microtubule tip. The beads bound to the microtubule tip in 90% of the trials. Being attached, the XMAP215 coated beads were moving over several micrometers during both microtubule polymerization and depolymerization (Fig.5.1). In some trials, the beads detached or got stuck to the surface before the microtubule underwent disassembly. Some microtubules did not grow with the tip-coupled XMAP215 coated beads.

To quantify the bead movement without load, the DIC movies were recorded with the acquisition rate of 3 frames per second. The position of the microsphere was identified by a tracking program at each movie frame. The program calculated a cross-correlation

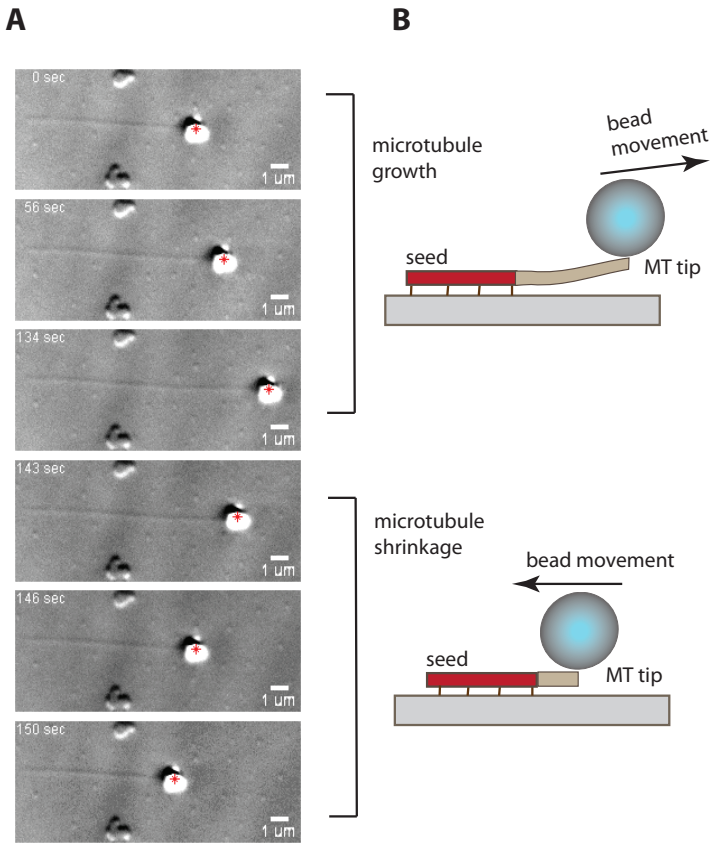

Figure 5.1: XMAP215 molecules harness microtubule energy to move a cargo. A. Some selected frames of the DIC movie of an XMAP215 coated bead moved by the polymerizing and depolymerizing microtubule end. The red cross, depicted at the images, represents the position of the bead defined by my tracking program. **B.** Schematic of my XMAP215 bead motility assay. A GMPCPP stabilized microtubule "seed" labeled with a rhodamine dye is attached to a glass surface via antibodies specific to the rhodamine dye. Upon addition of soluble unlabeled tubulin the microtubule "seed" start to grow and shrink. The XMAP215 bead remains attached to both growing and shrinking microtubule tip, following its leading edge.

coefficient between an image of the bead and each frame of the DIC movie. Based on the highest cross-correlation coefficient, the bead position was identified at each movie frame. Thus, the tracking program provides records of x and y coordinates of the bead position versus time. I rotated the coordinate system such that the microtubule was aligned along the y axis. If the microtubule is aligned along the y axis, then the bead movement due to the microtubule polymerization or depolymerization is represented by the y coordinate and the Brownian motion of the bead and lateral fluctuations of the microtubule are represented by the x coordinate. Some examples of the movement of

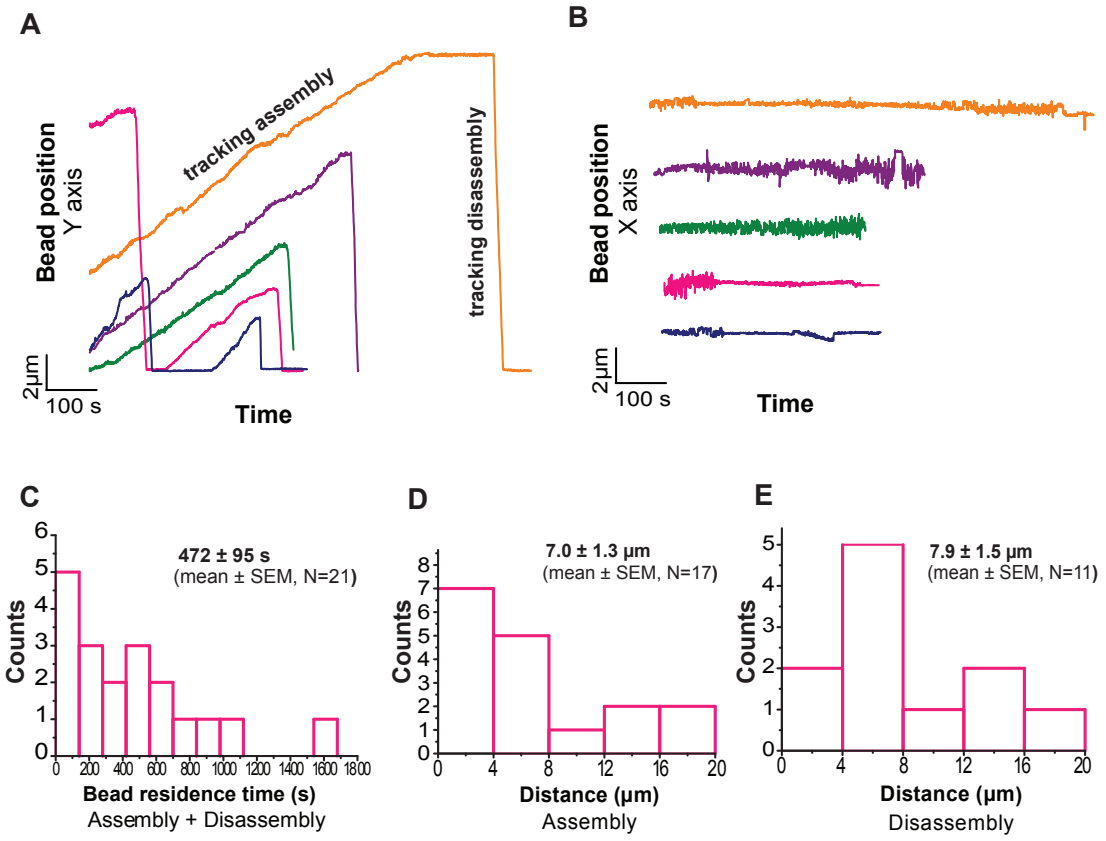

Figure 5.2: An XMAP215-coated bead travels several micrometers remaining attached to the microtubule tip during its assembly and disassembly. **A.** Records of the position of the XMAP215-coated beads versus time driven by the microtubule assembly and disassembly. The bead moves slowly when it is driven by microtubule assembly and fast during microtubule disassembly. **B.** Records of lateral movement of the XMAP215-coated beads driven by their Brownian motion and lateral fluctuations of the microtubules. **C.** Histogram of the bead residence time at the microtubule tip during both its assembly and disassembly. **C.** Histogram of the distances over which the XMAP215-coated beads moved powered by microtubule assembly. **E.** Histogram of the distances over which the XMAP215-coated beads moved powered by microtubule disassembly. In the top right corner of each histogram, the mean value is reported (mean ± SEM).

XMAP215-coated beads driven by the microtubule assembly and disassembly are illustrated on Fig. 5.2 A.

Neglecting the Brownian motion component and analyzing the traces of the XMAP215 bead movement due to the microtubule assembly or disassembly, I found that in the presence of 15 µM of tubulin and at 29 ℃, the XMAP215 beads, on average, remained

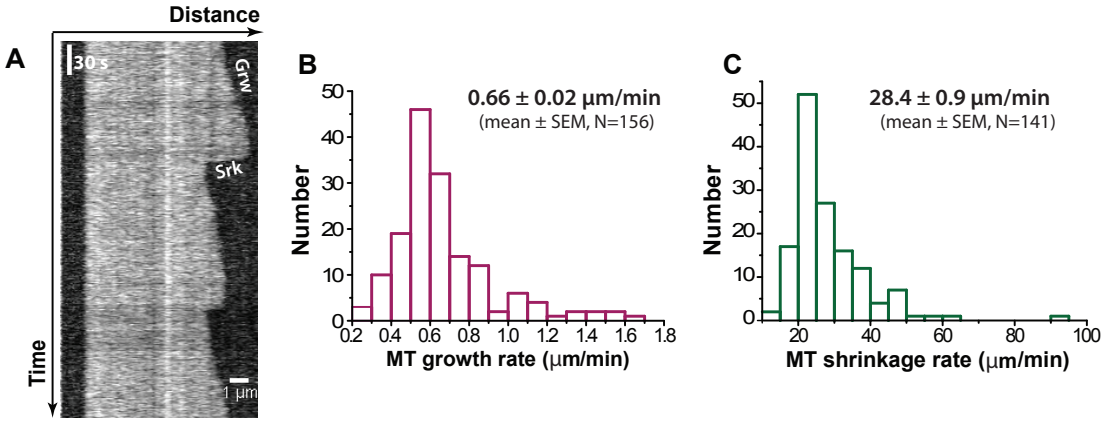

Figure 5.3: Growth and shrinkage speed of microtubules not associated with XMAP215-GFP coated beads. A. An example kymograph of a microtubule. The microtubule on the kymograph is depicted in light gray color. The growth phase is denoted by **Grw** and the shrinkage phase by **Shr**. The vertical bar represents 30 s and the horizontal bar represents 1 µm. **B.** Histogram of the microtubule growth speed calculated from the slopes of the microtubule growth phases of the kymographs. **C.** Histogram of the microtubule shrinkage speed calculated from the slopes of the microtubule shrinkage phases.

attached to the dynamic microtubule tip for 472 ± 95 s (mean ± SEM, N=21) (Fig. 5.2 C). During the attachment time they moved due to microtubule assembly, on average, over 7 ± 1.3 µm (mean ± SEM, N=17) before they either detached or switched to disassembly driven movement (Fig. 5.2 D). They moved, on average, over 7.9 ± 1.5 µm (mean ± SEM, N=11) due to the microtubule disassembly (Fig. 5.2 E). Therefore, XMAP215 molecules can maintain persistent attachment of a polystyrene microsphere, representing a cargo in my assay, to the microtubule growing and shrinking end. Because of this tip coupling, the bead travels along several micrometers during the microtubule growth and shrinkage powered by the energy of the microtubule polymerization and depolymerization. Hence, the XMAP215 molecules enable to harness the microtubule energy to move cargo.

5.2 XMAP215 molecules coupled to the polystyrene bead facilitate microtubule growth

XMAP215 is a polymerase that promotes microtubule growth. Therefore, a question arises whether XMAP215 molecules tagged with GFP and coupled to a polystyrene bead can promote microtubule growth as well. To address this question, I compared growth and shrinkage velocities of the microtubule tips that were not coupled to the XMAP215-GFP beads with the velocities of the XMAP215-coated beads driven by the microtubule assembly and the disassembly.

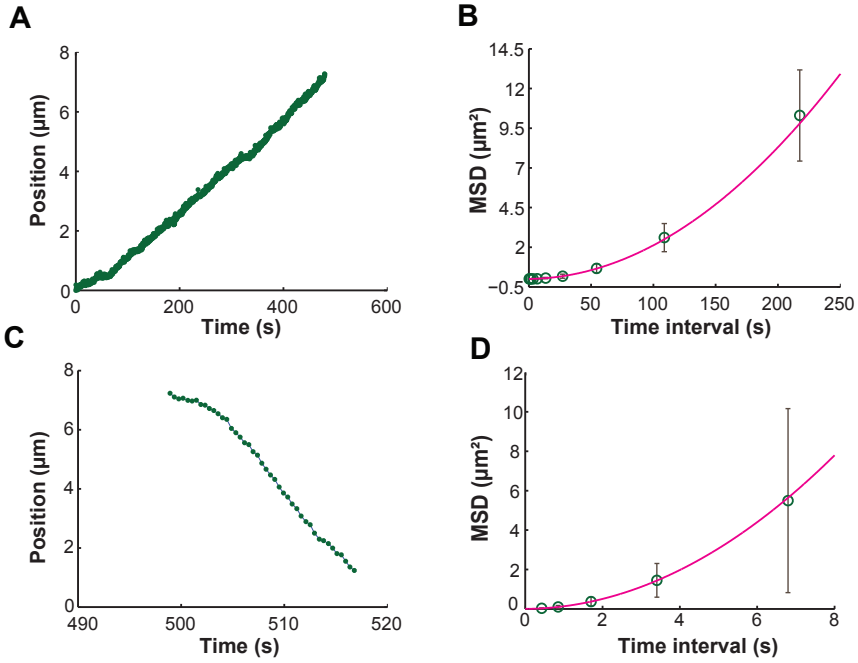

Figure 5.4: Calculation of the mean-squared displacement (MSD) of the XMAP215 coated beads driven by microtubule polymerization and depolymerization. **A.** Plot of the position of a XMAP215-coated bead versus time. The bead is driven by the microtubule assembly. **B.** Plot of the mean-squared displacement (MSD) of the bead following the microtubule polymerization versus time interval (green open circles). The error bars represent SEM. The data was fitted with a parabola $< \Delta y^2 >= at^2 + bt + c,\ a > 0, b > 0, c > 0$ (magenta line). **C.** Plot of the position of a XMAP215-coated bead versus time. The bead is driven by microtubule disassembly. **D.** Plot of the mean-squared displacement (MSD) of the bead following the microtubule depolymerization versus time interval (green open circles).

The growth and the shrinkage speeds of microtubules that were not interacting with the XMP215 beads were calculated from the DIC movies. In these movies, one could see in the same field of view the microtubule that had a XMAP215 bead at its plus-end and microtubules, which grew and shrunk without any interaction with a bead. The comparison of the speeds of the growth and the shrinkage of these microtubules with the speed of the bead movement ensures the same experimental conditions for both.

Usually, to quantify the dynamics of the microtubules, kymographs are produced. A kymograph illustrates how the microtubule length changes over time, where the horizontal axis represents distance and the vertical axis represents time. Therefore, in such a representation the microtubule dynamic end forms a saw-tooth pattern. The slopes of a

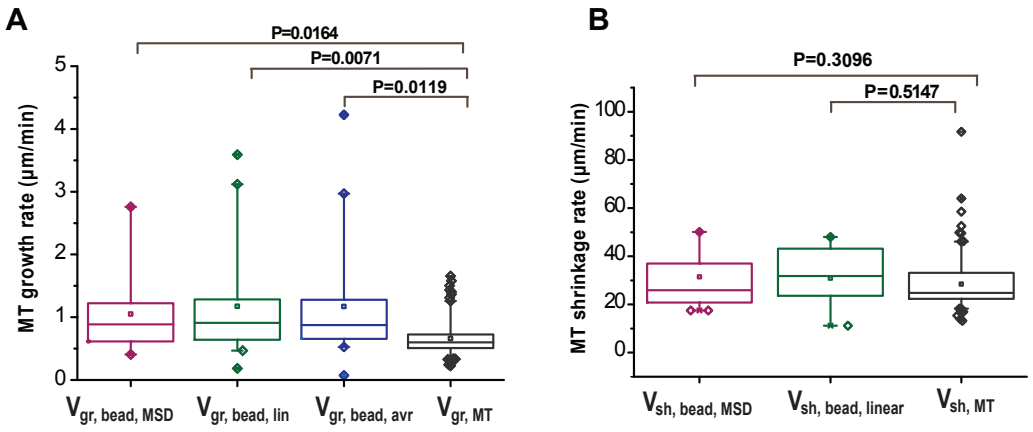

Figure 5.5: Comparison of the growth speeds of microtubules not interacting with XMP215-coated beads with the ones having tip-coupled XMAP215-coated beads. A. Box plots of the microtubule growth speeds with a tip-coupled bead (magenta, green, blue boxes) and the microtubule not interacting with a bead (black box). The growth speeds of the microtubules with tip-coupled beads were calculated in three ways and depicted by different colors: the magenta box plot represents the microtubule growth speed calculated from the MSD; the green box plot represents the microtubule growth speed calculated by the linear fit to the bead position record; the blue box plot represents the average microtubule growth speed. **B.** Box plots of the microtubule shrinkage speeds with a tip-coupled bead (magenta, green boxes) and the microtubule not interacting with a bead (black box).The shrinkage speeds of the microtubules with tip-coupled beads are calculated in two ways and depicted by different colors: the magenta box plot represents the microtubule growth speed calculated from the MSD; the green box plot represents the microtubule growth speed calculated by a linear fit to the bead position record.

"tooth" give the values of the microtubule growth and shrinkage speeds. However, due to a very small lateral size (25 nm) the images of the microtubule ends have poor contrast in DIC movies. As a consequence, it is not possible to distinguish the microtubule end from the background in the kymograph. To increase the contrast of the DIC movies, I processed them using Fiji (http://fiji.sc/wiki/index.php/Fiji). First, the movies were smoothed with a band-pass filter and then processed with an edge detection algorithm implemented in Fiji. This algorithm finds the microtubule edges and marks them brighter than the background enhancing their contrast. From such contrast-enhanced movies, I made the kymographs and calculated the microtubule growth and shrinkage speeds. An example of the obtained kymographs is illustrated in Fig.5.3 A.

The kymograph analysis showed that, in the presence of 15 µM of tubulin and at 29 ℃, the microtubules grew and shrunk with a speed of 0.66 ± 0.25 µm/min (mean ± SD, N=156) (Fig. 5.3 B.) and 28.4 ± 10.7 µm/min (mean ± SD, N=141) (Fig.5.3 C.),

Table 5.1: Velocities of the beads transported by polymerizing and depolymerizing microtubules calculated by different methods

Velocity (μm/min)	**Value (mean ± SEM, N)**
$V_{gr,bead,MSD}$	1.05 ± 0.14, N=17
$V_{gr,bead,lin}$	1.2 ± 0.2, N=24
$V_{gr,bead,avr}$	1.2 ± 0.2, N=24
$V_{sh,bead,MSD}$	31.4 ± 2.8, N=16
$V_{sh,bead,lin}$	30.9 ± 3.5, N=11

respectively.

The bead velocity was determined from the bead traces obtained by tracking the bead position in the DIC movies. Since the microtubule growth, in many cases, was not smooth, because of the events of rescue, and the microtubule growth speed could change during one growth phase, the bead movement could not be well described by linear dependence of the bead position on time. To overcome this problem, I calculated the speed of the bead movement in three different ways: i) by fitting the position data to a line and obtaining the slope of it, what represents the bead velocity; ii) by calculating the average velocity, namely dividing the displacement through which the bead moved by total time; iii) by calculating the mean-squared displacement (MSD) of the bead and fitting the MSD data to a parabola $< \Delta y^2 >= at^2 + bt + c,\ a > 0, b > 0, c > 0$, where a represents the squared velocity of the bead. The idea behind this approach is that since the bead moves directionally, driven either by the microtubule polymerization or depolymerization, the MSD plotted versus increasing time intervals can be described by the diffusion with drift equation: $< \Delta y^2 >= V^2\Delta t^2 + 2D\Delta t + 2\epsilon^2$, where V is a velocity of the bead movement, D is a diffusion term describing the random bead movement back and forth due to the quick microtubule polymerization and subsequent depolymerization, not leading to the catastrophe, but also not leading to the net increase in the bead displacement, and $2\epsilon^2$ is experimental measurement noise (Fig. 5.4) [45]. Thus, by fitting the MSD data to a parabola with the parameters a, b, and c being positive, one can deduce from the fit parameters the bead movement speed as $V = \sqrt{a}$. The values of the mean velocities of the bead movement due to the microtubule polymerization and depolymerization for all three cases are presented in Table 5.1. The comparison of these velocities, obtained by the different methods, gave a statistically insignificantly difference according to Welche's unpaired t-test. Therefore, the above described ways of the bead velocity calculation gave essentially the same result.

The comparison of the velocities of the beads, transported by polymerizing microtubules, $V_{gr,bead,MSD}$, $V_{gr,bead,lin}$, $V_{gr,bead,avr}$, with the growth speed of the microtubules not interacting with the microspheres by Welche's unpaired t-test gave the two-tailed p-

values of 0.016, 0.007, and 0.012, respectively. These p-values indicated that XMAP215 molecules coupled to a polystyrene bead increased the microtubule growth speed up to two fold. However, the comparison of the velocities of the beads transported by depolymerizing microtubules, $V_{sh,bead,MSD}$ and $V_{sh,bead,lin}$, with the shrinkage speed of the microtubules not interacting with the microspheres by Welche's unpaired t-test gave the two-tailed p-values of 0.3096 and 0.5147, respectively. Such p-values implied that the XMAP215-coated microspheres did not affect the microtubule depolymerization speed (Fig.5.5).

5.3 Being under load, XMAP215 molecules are able to harness microtubule energy of polymerization and depolymerization

To see whether XMAP215 molecules were able to support load and harness microtubule energy to move a cargo, I applied an increasing compressive force in my bead assay. For this purpose, an XMAP215 coated bead coupled to a microtubule tip was held constantly in a stationary optical trap. When the microtubule tip grew, the bead was moved away from the center of the optical trap and experienced an increasing compressive force (Fig.5.6 (A)). Upon reaching a certain compressive force, the XMAP215-coated bead detached from the microtubule tip. For the quantification of the detachment force, the position of the trapped bead over time was obtained with the sampling rate of 40000 Hz and recorded with a decimation factor of 50. The bead position was monitored by back-focal-plane interferometry. The microtubules grew in the presence of 7.5 µM tubulin and at 29 ℃.

The bead movement can be represented as a superposition of three motions: one is due to the growth of a microtubule tip, one due to lateral fluctuations of the microtubule, and one due to Brownian motion of the bead. To decompose the movement, the obtained data was rotated. After the rotation, the bead movement due to the microtubule polymerization was represented along the axis Y and its motion due to lateral fluctuations of the microtubule end was represented along the X axis (Fig.5.6 (B, C)).

After analysis of the bead movement in the stationary optical trap I concluded that the detachment force of the XMAP215-coated beads, used in my assay, was 1 ± 0.1pN (mean ± SEM, N=18) (Fig. 5.6 (D)). Hence, the XMAP215 molecules are able to support compression up to 1pN and harness microtubule energy to move the cargo, represented by the bead in my assay.

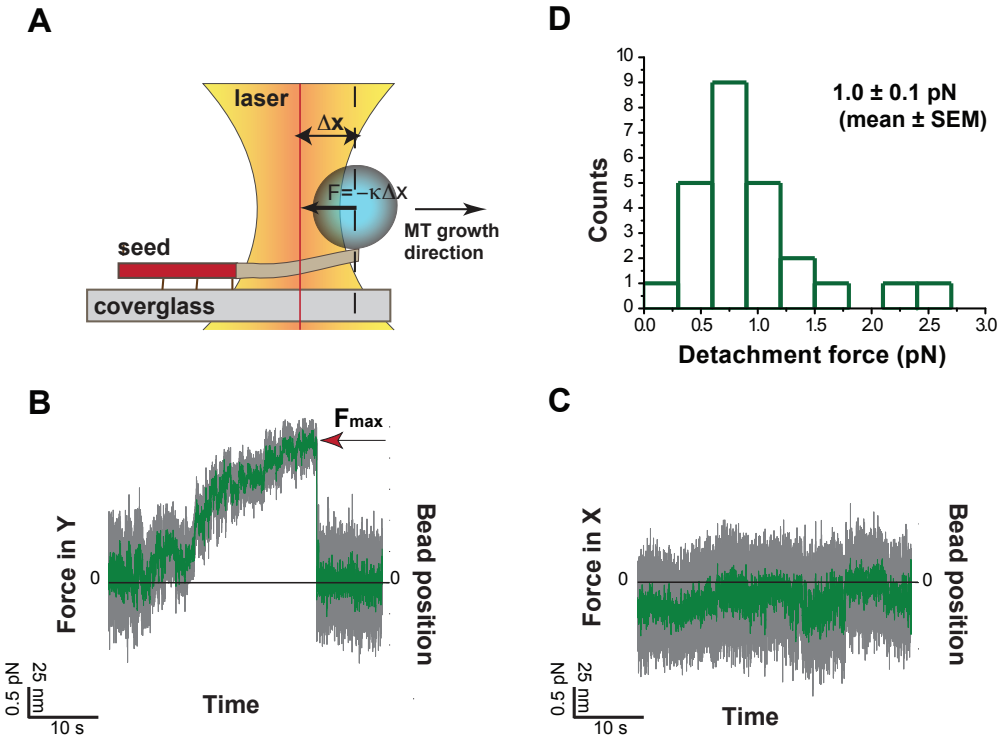

Figure 5.6: XMAP215 coated beads remain attached to the microtubule tip when compression is applied. A. Schematic of my bead assay with an applied increasing compressive force. **B.** The plot of the Y coordinate of the rotated bead position record versus time, representing the bead movement due to the microtubule growth (grey). Adjacent averaging of 100 data points is shown in green. The red arrow indicates a detachment of the bead from a microtubule tip. **C.** .The plot of the X coordinate of the rotated bead position record versus time, representing the Brownian motion of a bead (grey). The plot of the averaged Brownian motion of the bead versus time (green). **D.** Histogram of the maximal compressive forces that XMAP215-coated bead could support.

5.4 The force, applied towards microtubule growth, assists microtubule polymerization

The next question which I asked was whether the microtubule growth speed was tension sensitive. First, I investigated the effect of force pulling an XMAP215 coated bead coupled to a microtubule tip toward the direction of the microtubule growth. In this experiment, the force was kept constant by using a feedback-controlled mirror moving the position of an optical trap to maintain a fixed offset between the bead and the trap center (Fig. 5.7 (A)). The position of the bead was monitored by back-focal-plane in-

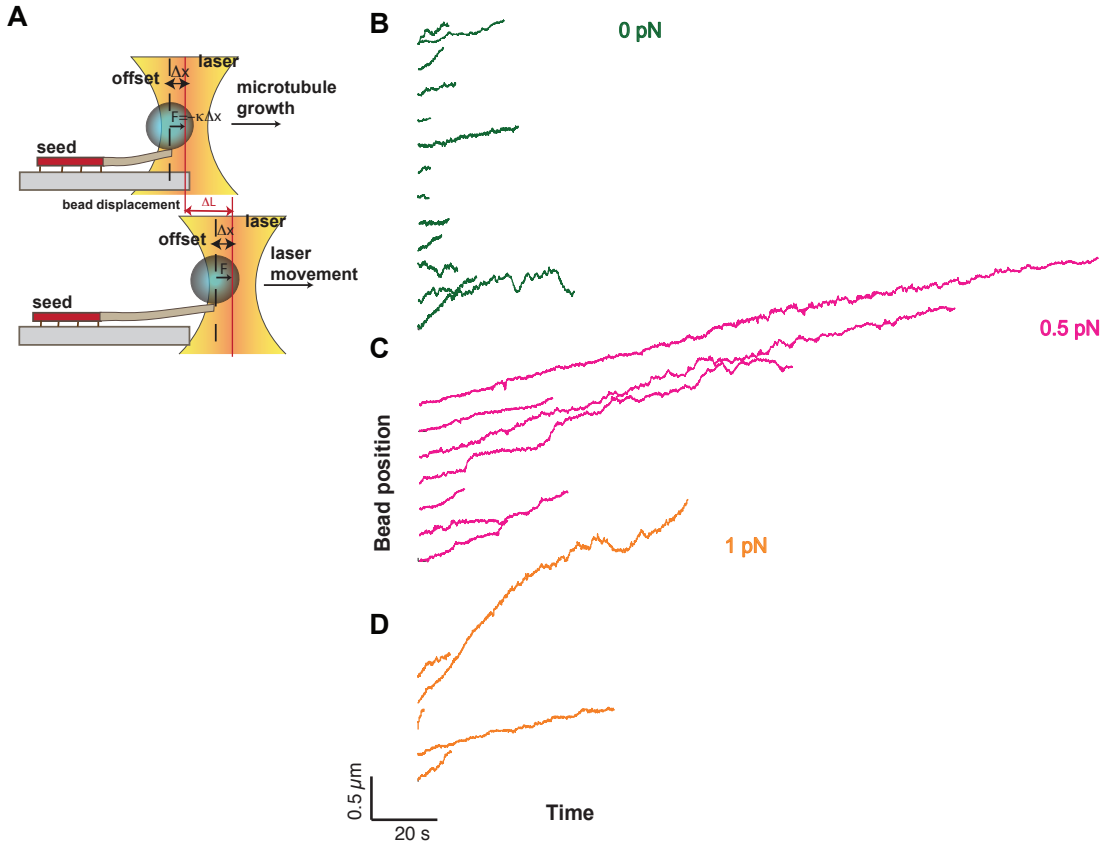

Figure 5.7: Records of the position of an XMAP215 coated bead coupled to a microtubule tip and subjected to a force applied in the direction of microtubule growth versus time. **A.** Schematic representing the experimental geometry and an application of a constant force pointing towards the direction of the microtubule growth. **B-D.** Records of the position of XMAP215 coated beads, coupled to a microtubule tip subjected to the force of 0pN (**B**), 0.5 pN (**C**), and 1 pN (**D**) applied in the direction of the microtubule growth versus time.

terferometry. The data was obtained with the sampling rate of 40000 Hz and recorded with a decimation factor of 10. The microtubules grew in the presence of 7.5 µM tubulin at 29 °C.

The speed of the bead movement with the applied forces of 0.5 pN and 1 pN was compared with the one without applied force. For this purpose, I followed the bead, held in the optical trap, both with and without applied force and obtained the records of the bead position versus time (Fig. 5.7 (B-D)). The bead position records were rotated and averaged over correlation time τ_{cor}, equal to 1.6 ms.The correlation time τ_{cor} is the trap relaxation time, equal to $\frac{1}{2\pi f_c}$, where f_c is the corner frequency of the power spectrum of an optical trap. The mean-squared displacement (MSD) was calculated and fitted to

a parabola, $< \Delta y^2 >= a\Delta t^2 + b\Delta t + c,\ a > 0, b > 0, -\infty < c < +\infty$, starting from 50 ms time interval, because in shorter time interval bead diffusive movement dominates over its directional movement (Fig. 5.8 (A-B). Different modes of the bead movement can be distinguished by the different slope values in log-log plot of MSD versus time interval (Fig. 5.8 (C)) . The MSD can be described by the diffusion-with-drift equation: $< \Delta L^2 >= V^2\Delta t^2 + 2D\Delta t + 2\delta^2 - \frac{2}{3}D\tau_{cor}$, where V is the velocity of the bead movement, D is a diffusion term describing the random bead movement back and forth due to the quick microtubule polymerization and the subsequent depolymerization, not leading to the catastrophe, but also not leading to the net increase in the bead displacement. The term $2\delta^2 - \frac{2}{3}D\tau_{cor}$ is experimental measurement noise, where δ is the tracking accuracy, and $\tau_{cor} = 1.6$ms is the correlation time [45] [102].

Based on the MSD analysis, when no force was applied, the XMAP215-coated bead moved with a speed of 0.59 ± 0.06 µm/min (mean ± SEM, N=11), and the bead placed under load of 0.5 pN and 1 pN moved with the velocities of 0.78 ± 0.06 µm/min (mean ± SEM, N=7) and 1.15 ± 0.29 µm/min (mean ± SEM, N=5), respectively (Fig. 5.8 (D)). To compare the velocity values, I did the unpaired Welch's t-test. The two-tailed p values of difference between the speeds of beads experiencing no load and placed under the load of 0.5pN and 1 pN were 0.0449 and 0.1409, respectively. According to these p value, V_{0pN} and $V_{0.5pN}$ are statistically different and V_{0pN} and V_{1pN} are not. In the latter case, the absence of the statistically significant difference can be explained, perhaps, by the small number of the measurements with 1pN applied force. Therefore, I concluded that the force, applied in the direction of microtubule growth to the microtubule tip-coupled bead, promotes microtubule growth.

From the same MSD analysis I also deduced the values of the diffusion coefficient, experimental noise measurement, and tracking accuracy (Fig. 5.8 (E-G)). Beads moved with a diffusion coefficient, D, of (0.46 ± 0.02)·10^{-3} µm^2/s (mean ± SEM, N=13) when no force was applied, and of (0.29 ± 0.02)·10^{-3} µm^2/s (mean ± SEM, N=7) and of (0.31 ± 0.06)·10^{-3} µm^2/s (mean ± SEM, N=5) when they were placed under tension of 0.5 pN and 1 pN, respectively. To compare the value of diffusion coefficients of the beads moving without external load with the ones with load of 0.5 pN and 1 pN, I did the unpaired Welch's t-test and obtained two-tailed p values of less than 0.0001 and 0.0596, respectively. Therefore, the difference between D_{0pN} and $D_{+0.5pN}$ is statistically significant, and the difference between D_{0pN} and D_{+1pN} is not (Fig. 5.8 (E)). In the latter case, the absence of the statistically significant difference can be explained, perhaps, by the small number of the measurements with 1pN applied force. Hence, I concluded that the force, applied in the direction of microtubule growth to the microtubule tip-coupled bead, decreases the diffusion coefficient of the beads and inhibits their diffusive movement.

The noise measurement, $c = 2\delta^2 - \frac{2}{3}D\tau_{cor}$, was (0.08 ± 0.02)·$10^{-4}$ µm^2 (mean ± SEM, N=13), (0.10 ± 0.03)·10^{-4} µm^2 (mean ± SEM, N=7), and (0.11 ± 0.03)·10^{-4} µm^2 (mean

± SEM, N=13) for the tension of 0 pN, 0.5 pN and 1pN, respectively. This gave the tracking accuracy, δ, of approximately, 2nm (Fig. 5.8 (F,G)).

5.5 The force, applied in the direction of microtubule growth, decreases both the on-rate and off-rate of tubulin dimers at the microtubule end

XMAP215 molecules attached to a bead couple the bead to a microtubule tip. Because the molecules maintain persistent attachment to both the growing and the shrinking microtubule tip, the bead gets transported by the polymerizing and depolymerizing microtubule end. Microtubules polymerize by addition and depolymerize by removal of tubulin dimers from their ends. To be transported, the XMAP215 coated bead has to be at the very tip of the growing or shrinking microtubule. Hence, knowing the position of the bead one can know the position of the microtubule tip. Therefore, by analyzing the records of the bead position versus time, one can deduce how many tubulin dimers were added or removed from the microtubule tip during bead movement. By sensing the position of the tip-coupled bead, I can detect the on-rate and the off-rate of the tubulin dimers.

The on-rate, k_{on}, and the off-rate, k_{off}, of the tubulin dimers at the microtubule end can be directly calculated from the mean-squared displacement of the tip-coupled bead [45]. The MSD of the bead can be decomposed into two components. One is the diffusion component $< \Delta l_d^2 >= 2D\Delta t$ due to the quick association and dissociation of the tubulin dimers from the microtubule tip and the other one, $< \Delta l_p^2 >= V^2\Delta t^2$, is the directed transport of the tip-coupled bead by the polymerizing microtubule.

According to [105][94][45], the microtubule growth rate variance can be represented as

$$< \Delta l_d^2 >= \xi^2(k_{on}[Tub] + k_{off})\Delta t.$$

Hence, the diffusion coefficient, D, is given by

$$D = \frac{\xi^2}{2}(k_{on}[Tub] + k_{off}).$$

The microtubule growth speed by definition is:

$$V_{gr} = \xi(k_{on}[Tub] - k_{off}),$$

where ξ is a change in the microtubule length contributed by the addition of one tubulin dimer, and it is equal to $\sigma/N = 0.615$ nm, where $\sigma = 8$ nm corresponds to the size of tubulin dimer and N = 13 corresponds to the number of protofilaments, $[Tub]$ is the tubulin concentration. Therefore, combining the last two equations, the on-rate, k_{on},

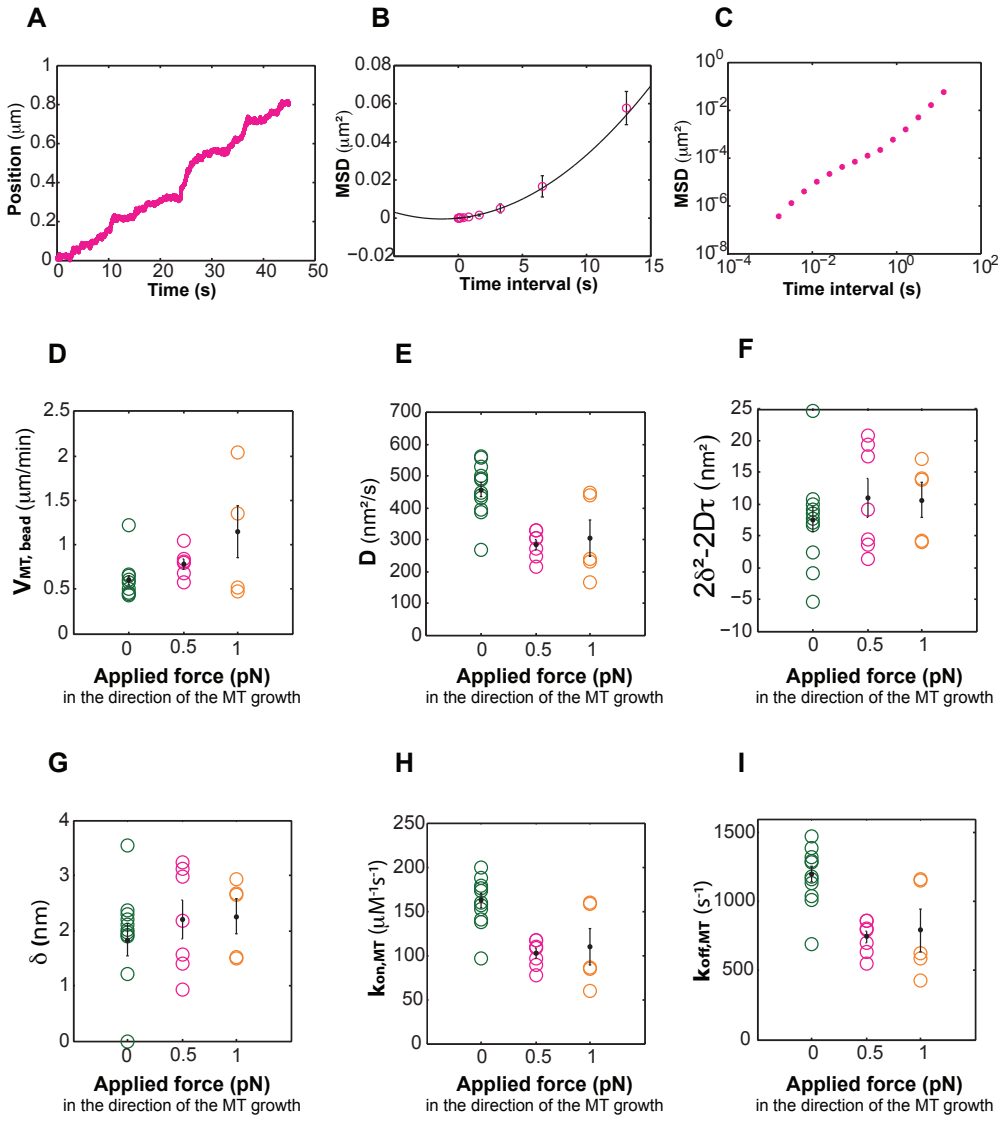

Figure 5.8: Mean-squared displacement analysis of records of the positions of beads transported by a polymerizing microtubule and subjected to an external force pointing in the direction of microtubule growth, versus time. **A.** A record of position of a bead coupled to a polymerizing microtubule tip and subjected to the external constant force of 0.5 pN. **B.** Mean-squared displacement (MSD) of the bead from the trace depicted in A. (open magenta circles) and the parabola fit to the MSD (black line). The error bars represent SEM. **C.** Log-log plot of MSD from the trace depicted in A. versus time interval **D.** The dependence of the microtubule growth speed, V_{gr}, on the force applied in the direction of the microtubule growth. **E.** The dependence of the diffusion coefficient, D, on the force applied in the direction of the microtubule growth. **F.** The dependence of the noise measurement, $c = 2\delta^2 - 2D\tau$, $\tau = \tau_{cor}/3$, on the force applied in the direction of the microtubule growth. **G.** The dependence of the tracking accuracy, δ, on the force applied in the direction of microtubule growth. **H.** The dependence of the on-rate of tubulin dimers, k_{on}, at the microtubule end on a force applied in the direction of microtubule growth. **I.** The dependence of the off-rate of tubulin dimers, k_{off}, at the microtubule end on a force applied in the direction of microtubule growth. **(D-I)** Black dots represent the means and the error bars are SEMs.

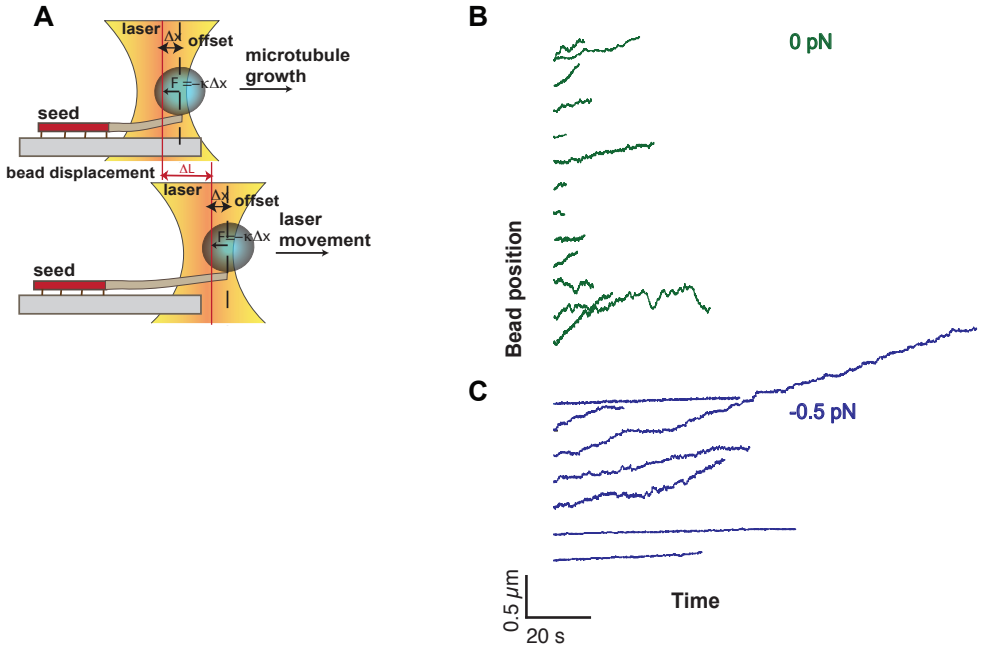

Figure 5.9: Records of the position of a XMAP215-coated bead, coupled to a microtubule tip and subjected to a force applied against microtubule growth versus time. A. Schematic representing the experimental geometry and an application of a constant force pointing against the direction of microtubule growth. **B.** Records of the position of a XMAP215-coated bead coupled to a microtubule tip with no applied force versus time. **C.** Records of the position of a XMAP215-coated bead coupled to a microtubule tip and subjected to the force of 0.5 pN opposing the microtubule growth versus time.

and the off-rate, k_{off}, of the tubulin dimers are given by:

$$k_{on} = \frac{2D + \xi V_{gr}}{2\xi^2 [Tub]},$$

$$k_{off} = \frac{2D - \xi V_{gr}}{2\xi^2}.$$

The diffusion coefficient, D, and the microtubule growth speed, V_{gr}, can be estimated from the parabola fit to the MSD of the microtubule tip-coupled bead versus time interval.

To see how the on-rates and off-rates of the tubulin dimers at the microtubule end depended on force, I calculated their values at the different applied forces. On average, the on-rate rate, k_{on}, was 162 ± 8 μM^{-1} s^{-1} (mean ± SEM, N=13), 102 ± 6 μM^{-1}

s^{-1} (mean ± SEM, N=7) and 110 ± 21 μM^{-1} s^{-1} (mean ± SEM, N=5) for 0 pN, 0.5 pN and 1 pN forces, respectively. According to Welche's unpaired t-test, the tubulin on-rates at the microtubule end $k_{on,0pN}$ and $k_{on,+0.5pN}$ were significantly different with a two-tailed p value of 0.0001, whereas $k_{on,0pN}$ and $k_{on,+1pN}$ were not significantly different (p = 0.0644), possibly, because of the small number of the measurements with applied force of 1 pN. Thus, the on-rate of the tubulin dimers decreased when the XMAP215 molecules were under the load.

The off-rate, k_{off}, on average, was 1199 ± 59 s^{-1} (mean ± SEM, N=13), 745 ± 44 s^{-1} (mean ± SEM, N=7) and 792 ± 152 s^{-1} (mean ± SEM, N=5) for 0 pN, 0.5 pN and 1 pN forces, respectively (Fig. 5.8 (H, I)). According to the Welche's unpaired t-test, the tubulin off-rates at the microtubule end $k_{off,0pN}$ and $k_{off,+0.5pN}$ were significantly different with a two-tailed p value of 0.0001, whereas $k_{off,0pN}$ and $k_{off,+1pN}$ were not significantly different (p = 0.0551), possibly, because of the small number of the measurements with applied force of 1 pN. Therefore, the off-rate of the tubulin dimers at the microtubule end also decreased when there was a load applied on the XMAP215 molecules.

5.6 A force opposing microtubule growth, does not affect microtubule polymerization rate

To test the effect of a force reversal on the microtubule growth speed, I applied a constant force of 0.5 pN opposing microtubule growth (Fig. 5.9). The data was collected and analyzed as described above in sec. 5.4. From the records of the bead position versus time, I calculated the MSD of the bead. The MSD was fitted to a parabola, and the microtubule growth speed was calculated from the fitting parameters (Fig. 5.10 (A-C)). With an applied force of –0.5 pN, the microtubule growth speed was 0.53 ± 0.01 µm/min (mean ± SEM, N=7) (Fig. 5.10 (D)). When no force was applied, the microtubule growth speed was 0.59 ± 0.06 µm/min (mean ± SEM, N=13). The comparison of the bead velocities V_{0pN} and $V_{-0.5pN}$ by the Welche's unpaired t-test, gave a two-tailed p value of 0.2818. This implied that there was no change in the bead velocity when the 0,5 pN opposing force to the microtubule growth is applied. Hence, the force opposing microtubule growth did not influence the speed of microtubule polymerization.

The diffusion coefficient, D, was (0.46 ± 0.02)·10^{-3} $\mu m^2/s$ (mean ± SEM, N=13) and (0.27 ± 0.01)·10^{-3} $\mu m^2/s$ (mean ± SEM, N=7) for 0pN and 0.5 pN force applied, respectively (Fig. 5.10 (E)). The comparison of the diffusion coefficients according to the Welch's unpaired t-test gave a p-value of 0.0001. This indicated that the diffusion coefficient with no load and the one with 0.5 pN opposing load to the microtubule growth are significantly different. Therefore, the force opposing to the microtubule growth decreased the bead diffusion coefficient.

The noise measurement, $c = 2\delta^2 - \frac{2}{3}D\tau_{cor}$, was (0.08 ± 0.02)·$10^{-4}$ μm^2 (mean ± SEM,

N=13) and $(0.53 \pm 0.02) \cdot 10^{-5}$ µm^2 (mean ± SEM, N=7) for the tension of 0 pN and – 0.5 pN, respectively. This gave the tracking accuracy, δ, approximately, 2nm (Fig. 5.10 (F,G)).

5.7 A force opposing microtubule growth decreased both the on-rate and off-rate of tubulin dimers at the microtubule end

To test the influence of an opposing force on the on-rate and off-rate of the tubulin dimers at the microtubule end, I estimated their values from the parabola fit to the MSD of the microtubule tip-coupled bead placed under load and without any load. The on-rate of the tubulin dimers, k_{on} was 98 ± 2 µM^{-1} s^{-1} (mean ± SEM, N=7) and the off-rate of the tubulin dimers, k_{off}, was 718 ± 18 $^{-1}$ (mean ± SEM, N=7). The on-rate and off-rate with no force applied was 162 ± 8 µM^{-1} s^{-1} (mean ± SEM, N=11) and 1199 ± 59 s^{-1} (mean ± SEM, N=11), respectively (Fig.5.10 (G, H)).

According to the Welche's unpaired t-test, the on-rate of tubulin dimers at the microtubule end with no force applied and 0.5 pN opposing force to the microtubule growth applied were significantly different (two-tailed p-value is 0.0001). The off-rates of the tubulin dimers at the microtubule end with no load and opposing load to the growth were also significantly different (two-tailed p-value is 0.0216). This implies that an external opposing force decreased both the on-rate and off-rate of tubulin dimers at the microtubule tip. The force influence on the off-rate was stronger. Interestingly, in comparison with the +0.5 pN force applied in the direction of microtubule growth, the opposing force hinders the loss and the addition of tubulin dimers more effectively.

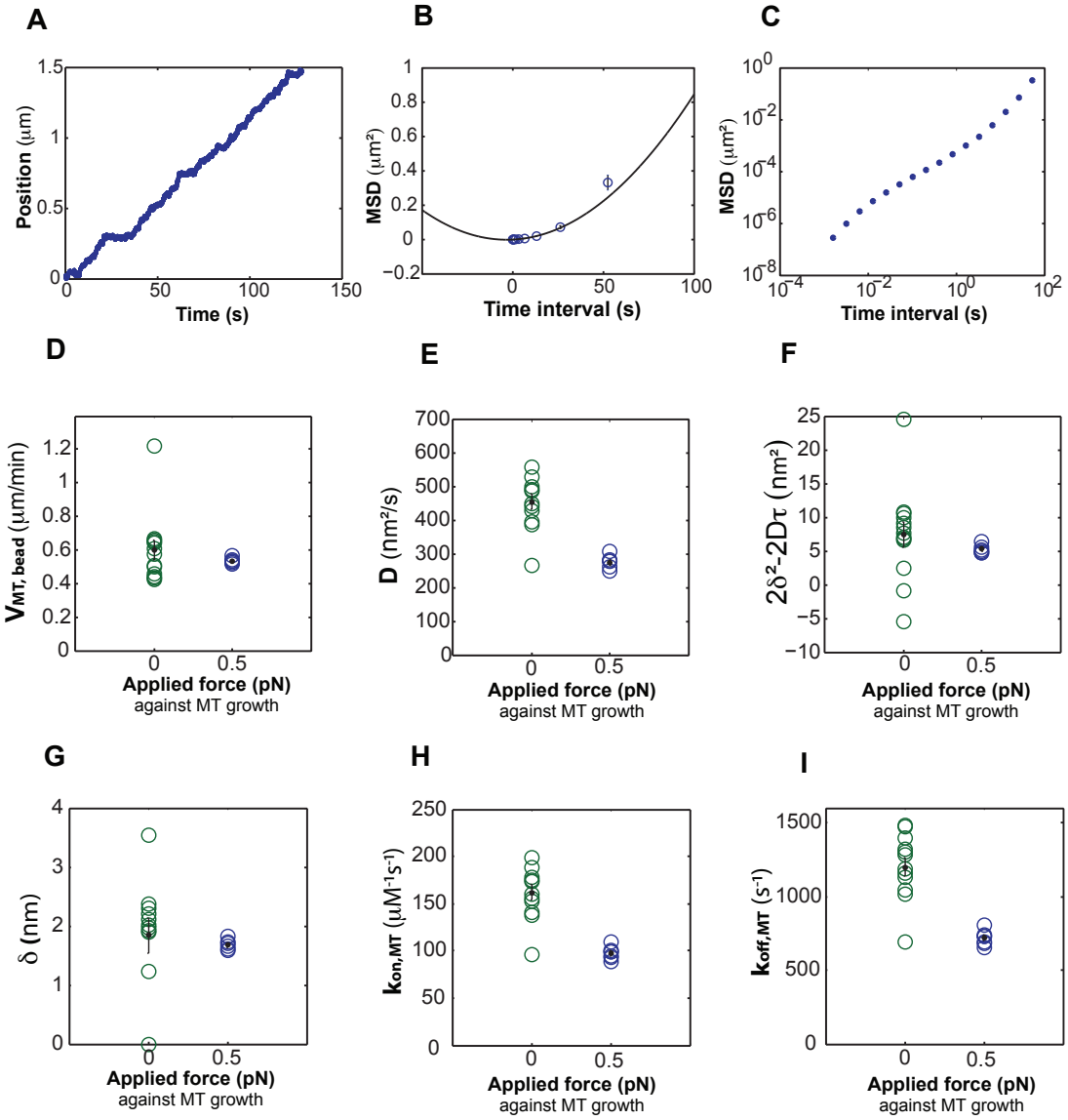

Figure 5.10: Mean-squared displacement analysis of records of bead position, transported by a polymerizing microtubule and subjected to an external force pointing against microtubule growth, versus time. A. A record of position of a bead coupled to a polymerizing microtubule tip and subjected to the external constant force of – 0.5 pN. **B.** Mean-squared displacement (MSD) of the bead from the trace depicted in A. (open blue circles) and the parabola fit to the MSD (black line). The error bars represent SEM. **C.** Log-log plot of MSD from the trace depicted in A. versus time interval **D.** The dependence of the microtubule growth speed, V_{gr}, on the applied force pointing against microtubule growth. **E.** The dependence of the diffusion coefficient, D, on the applied force pointing against microtubule growth. **F.** The dependence of the noise measurement, $c = 2\delta^2 - 2D\tau$, $\tau = \tau_{cor}/3$, on the applied force pointing against microtubule growth. **G.** The dependence of the tracking accuracy, δ, on the applied force pointing against microtubule growth. **H.** The dependence of the on-rate of tubulin dimers, k_{on}, at the microtubule end on the applied force pointing against microtubule growth. **I.** The dependence of the off-rate of tubulin dimers, k_{off}, at the microtubule end on the applied force pointing against microtubule growth. **(D-I)** Black dots represent the means and the error bars are SEMs.

Chapter 6

Discussion, Conclusions and Outlook

In my study, I coupled XMAP215 molecules to the polystyrene microsphere and looked at the interaction of several XMAP215 molecules with the microtubule plus-end. I also investigated the effect of a force applied to the XMAP215 molecules following microtubule growing end on the microtubule polymerization speed and the rates of the association and dissociation of tubulin dimers at the microtubule plus-end.

My experiments demonstrated that XMAP215 molecules can link cargo to the growing and shrinking end of a microtubule, allowing its transport over several micrometers. This property stems from the ability of XMAP215 molecules to bind and surf the growing and shrinking microtubule plus-end. Each, XMAP215 molecule remains associated with microtubule plus-end, on average, for 4s [22]. In my experiment, the XMAP215 molecules are coupled to the bead. The ratio of XMAP215 molecules per bead is such that several XMAP215 molecules interact with the microtubule plus-end at the same. In addition, because of the large size, the bead can not diffusive away from the microtubule plus-end fast, promoting successive attachments of the bead- coupled XMAP215 molecules. This increases the time of the microtubule tip interaction of the XMAP215-covered bead to 472 $\pm$ 95 s (mean $\pm$ SEM, N=21).

The fission and budding yeast, as well as *Drosophila* orthologues of XMAP215 are found to localize at the kinetochores [25, 43, 111], special structures maintaining attachment of the chromosomes to the microtubule tips during cell devision. Being at the kinetochores XMAP215 proteins nucleate microtubule and regulate microtubule plus-end dynamics. Therefore, the ability of persistent attachment of several XMAP215 molecules to the microtubule tip can be crucial for the XMAP215 function at the kinetochores, which can be thought as cargo.

So far, only Dam1 complex and Ndc80 were shown to harness energy of the microtubule polymerization and depolymerization to move cargo [10, 41, 96]. These molecules

also are associated with the kinetochores. Their function is to maintain the persistent attachment of the chromosomes to the microtubule tips. Beads covered with Dam1 complex maintain persistent attachment to the polymerizing and depolymerizing microtubule plus-ends for 180s ± 30 s [10]. It travels 2.4 ± 0.2 µm during microtubule polymerization before detachment and 3.4 ± 0.4 µm during microtubule depolymerization [10]. Ndc80- covered beads remain attached to the microtubule tips for 180 ± 30 s and travel over 4.8 ± 0.4 µm during microtubule depolymerization [96]. With applied external load, Ndc80-covered beads follow microtubule polymerization over 0.67 ± 0.07 µm [96]. My study suggests that XMAP215-covered beads have 2.5-fold longer residence time on the microtubule plus-end, 472 ± 95 s (mean ± SEM, N=21), and travel double distance of the one of the Dam1- or Nds-80-covered beads, 7 ± 1.3 µm (mean ± SEM, N=17) due to microtubule assembly and 7.9 ± 1.5 µm (mean ± SEM, N=11) due to microtubule disassembly.

XMAP215 is a processive polymerase [22]. Being coupled to the polystyrene microsphere, XMAP215 molecules increase microtubule growth speed two-fold. However, according to the *in vitro* studies of Brouhard et al. [22], the maximal increase in microtubule growth speed at saturated XMAP215 concentration is fivefold. How can this difference be reconciled? One possibility is that the number of bead tethered XMAP215 molecules interacting at the same time with the microtubule plus-end is not enough to increase the growth speed of all microtubule protofilaments [22]. The other possibility is that the polystyrene bead interferes with the XMAP215 molecules coupled to it inhibiting their polymerization activity.

One aspect of my studies is the force influence on the microtubule polymerization speed. Here, I showed that the 0.5 pN force applied to the XMAP215 molecules in the direction of microtubule growth increases the microtubule growth speed 1.3-fold and, therefore, enhances XMAP215 polymerization activity. Interestingly, the force of the same magnitude but applied in the direction opposite to microtubule growth does not affect the microtubule growth rate and the XMAP215 polymerization activity. One possibility is that because of the external force, the diffusion of XMAP215 molecules is reduced and the XMAP215-coated beads are favored to move in the direction of the external force. Now, if the external force is applied in the direction of the microtubule growth, the XMAP215-coated beads are constrained at the very tip of the microtubule, to which XMAP215 molecules have higher affinity than to the microtubule lattice. Being at the microtubule tip, XMAP215 molecules polymerize microtubule by incorporation of tubulin dimers into the protofilaments. On the contrary, if the external force points in the direction opposite to the microtubule growth favors leaving microtubule tip by the XMAP215-coated bead and XMAP215 molecules can not add tubulin dimers so effectively any more.

The diffusion coefficient of the XMAP215-covered bead was reduced 1.6-fold when 0.5 pN force was applied pointing in either direction. This is in agreement with the pos-

sible above discussed explanation of the force effect on the microtubule growth and/or XMAP215 polymerization activity.

The similar studies were performed with Ndc80 and Dam1 proteins [10, 41, 96]. The beads covered with Dam1 complex or Ndc80 could stand the load of 0.2-2.5 pN before their detachment from the microtubule. In case of Ndc80, the enhancement of microtubule growth speed was not observed [96]. However, in the study of Dam1 complex it was shown that one can promote microtubule growth by application of tension to the microtubule tip in the direction of its growth through the Dam1 linker. The explanation is that Dam1 complexes bound to the bead form a ring that encircles the microtubule tip. When the tension is applied in the direction of the microtubule growth, the Dam1 ring forces microtubule protofilaments to straight up. Thereby, it facilitates microtubule elongation by inhibiting microtubule catastrophe frequency, although it does not affect microtubule growth speed due to the lack of polymerization activity by itself [10]. The authors argued that this Dam1 ring ability can be important for the maintenance of the secure attachment of the chromosomes to the spindle microtubules via kinetochores. XMAP215 molecules do not form a complex. Therefore, when I applied tension to the XMAP215 molecules in either direction, I put under the tension not the microtubule tip, but rather the XMAP215 molecules. However, since XMAP215 molecules localize at the kinetochore in different organisms, the property of bearing load can be important for carrying out their functions at the kinetochores.

Since the microtubule growth speed is increased when an external force is applied in the direction of the microtubule growth, it is interesting to see how the rate of the addition and loss of tubulin dimers changes with applied tension. My experiments suggest that both the on-rate and off-rate of tubulin dimers are decreased 1.6- and 1.7-fold, respectively, when 0.5 pN force was applied in either direction. Therefore, the off-rate seems to be slightly more affected by the force than the on-rate of tubulin dimers.

The on-rate and off-rate of the tubulin dimer that I obtained from my MSD analysis are 162 $\pm$ 8 µm $M^{-1}s^{-1}$ (mean $\pm$ SEM, N=13) and 1199 $\pm$ 59 s^{-1} (mean $\pm$ SEM, N=13) when there is no external load. In recent studies of the on- and off-rates of tubulin dimers at the microtubule end with total-internal-reflection-fluorescence microscopy, Gardner et al. reported the values for the on-rate of 58 $\pm$ 4 $\mu m^{-1}s^{-1}$ and the predicted off-rate of 450 s^{-1} at 7.5 µM tubulin [45]. Such a difference in on- and off-rate can indicate the XMAP215 polymerization activity. On other hand, it can be explained by the fact that in my calculation of on- and off-rates of the tubulin dimers at the microtubule end was involved the diffusion coefficient, D, which contains the component of the diffusion of XMAP215 molecules over microtubule lattice and the variance in the length of the microtubule tip. Hence, it would be interesting to see wether one can obtained similar results to [45] if only the variation in the length of a microtubule tip is taking into the account.

Glossary

A_{tub}	tubulin absorbance at 280 nm
I	path length of the cuvette
C_{tub}	tubulin concentration
ϵ	extinction coefficient
A_{dye}	TAMRA absorbance at 555 nm
CF	correction factor to account for TAMRA absorbance at 280 nm
ϵ_{dye}	TAMRA extinction coefficient
A	absorption
D	size of the dielectric object
λ	wavelength
n_m	refractive index of the medium
n_o	refractive index of the object
θ_i	incident angle of the light ray
θ_r	refractive angle
F_{grad}	gradient force
F_{scat}	scattering force
R	microsphere radius
E	magnitude of electric field
U	potential
κ	stiffness
x	bead displacement
F	restoring force
F_{trap}	trapping force
Δx	bead displacement
β	sensitivity factor
S_0	plateau value in a Lorentzian-type power spectrum
f_c	corner frequency in a Lorentzian-type power spectrum
A	amplitude (p. 29)
P_{spike}	power spectral density of a spike at an oscillatory frequency
Δf	frequency interval
f_{oscil}	oscillation frequency
γ	drag coefficient
D	diffusion coefficient

k_b	Boltzmann constant
T	absolute temperature
$U(t)$	output signal
P	proportional gain
I	integral gain
D	derivative gain (p. 30-31)
e	error magnitude
τ	error duration
t	time
x_{bead}	bead position
x_{mirror}	mirror signal of bead position
x_{QPD}	QPD signal of bead position
$< \Delta y^2 >$	bead mean-squared displacement
V	bead movement velocity
ϵ^2	experimental noise
δ^2	tracking accuracy
τ_{cor}	correlation time
ξ	change in microtubule length contributed by an addition of one tubulin dimer
GTP	guanosine triphosphate
GDP	guanosine diphosphate
MAPs	microtubule associated proteins
ATP	adenosine triphosphate
Op18	oncoprotein 18
Ncd	non-claret disjunctional gene
Klp	kinesin-like protein
MAP1	microtubule associated protein 1
MAP2	microtubule associated protein 2
XMAP215	xenopus microtubule associated protein with a molecular weight of 215 kDa
EB	microtubule end-binding protein
CLIPs	cytoplasmic linker proteins
CLASPs	cytoplasmic linker associated proteins
ACP	adenomatous polyposis coli
MCAK	mitotic centromere-associated kinesin
chTOG	colonic, hepatic tumor over-expressed gene
Msps	mini-spindles
ZYG9	zygote defective gene
MOR1	microtubule organisation gene 1
Stu2	suppressors of a tubulin mutation 2
Dis1	defect in sister chromatid disjoining 1
Alp14	gene locus 14, altered polarity
TACC	transforming acidic coiled-coil
TOG	tumor overexpressed gene
HEAT	huntingtin, elongation factor 3, the PR65/A subunit of

	protein phosphatase 2A and the lipid kinase Tor
GFP	green fluorescent protein
His 7	7 histidines
TAMRA	tetramethylrhodamine dye
PCR	polymerase chain reaction
DIC	differential interference contrast
PEG	polyethylene glycol molecule
sulfo-NHS	N-hydroxysulfosuccinimide sodium salt
EDC	N-(3-dimethylaminopropyl)-N′-ethylcarbodiimide hydrochloride
DTT	dithiothreitol
DDS	dimethyldichlorosilane
TCE	trichloroethylene
GMPCPP	guanosine-5'-[(alpha,beta)-methyleno]triphosphate
PEO	poly(ethylene oxide)
PPO	poly(propylene oxide)

List of Figures

List of Tables

Bibliography

[1] A. Akhmanova and C. C. Hoogenraad. Microtubule plus-end-tracking proteins: mechanisms and functions. *Current Opinion in Cell Biology*, 17(1):47–54, Feb 2005.

[2] A. Akhmanova, C. C. Hoogenraad, K. Drabek, T. Stepanova, B. Dortland, T. Verkerk, W. Vermeulen, B. M. Burgering, C. I. D. Zeeuw, F. Grosveld, and N. Galjart. Clasps are clip-115 and -170 associating proteins involved in the regional regulation of microtubule dynamics in motile fibroblasts. *Cell*, 104(6):923–35, Mar 2001.

[3] A. Akhmanova and M. O. Steinmetz. Tracking the ends: a dynamic protein network controls the fate of microtubule tips. *Nat Rev Mol Cell Bio*, 9(4):309–22, Apr 2008.

[4] A. Akhmanova and M. O. Steinmetz. Microtubule +tips at a glance. *J Cell Sci*, 123(Pt 20):3415–9, Oct 2010.

[5] J. Al-Bassam. Stu2p binds tubulin and undergoes an open-to-closed conformational change. *The Journal of Cell Biology*, 172(7):1009–1022, Mar 2006.

[6] J. Al-Bassam and F. Chang. Regulation of microtubule dynamics by tog-domain proteins xmap215/dis1 and clasp. *Trends in cell biology*, Jul 2011.

[7] J. Al-Bassam, H. Kim, G. Brouhard, A. van Oijen, S. C. Harrison, and F. Chang. Clasp promotes microtubule rescue by recruiting tubulin dimers to the microtubule. *Developmental Cell*, 19(2):245–58, Aug 2010.

[8] J. Albassam, N. Larsen, A. Hyman, and S. Harrison. Crystal structure of a tog domain: Conserved features of xmap215/dis1-family tog domains and implications for tubulin binding. *Structure*, 15(3):355–362, Mar 2007.

[9] I. Arnal, C. Heichette, G. S. Diamantopoulos, and D. Chrétien. Clip-170/tubulin-curved oligomers coassemble at microtubule ends and promote rescues. *Curr Biol*, 14(23):2086–95, Dec 2004.

[10] C. L. Asbury, D. R. Gestaut, A. F. Powers, A. D. Franck, and T. N. Davis. The dam1 kinetochore complex harnesses microtubule dynamics to produce force and movement. *Proc Natl Acad Sci USA*, 103(26):9873–8, Jun 2006.

[11] A. Ashkin. Acceleration and trapping of particles by radiation pressure. *Physical Review Letters*, Jan 1970.

[12] A. Ashkin. Forces of a single-beam gradient laser trap on a dielectric sphere in the ray optics regime. *Biophysical Journal*, Jan 1992.

[13] J. Bechhoefer. Feedback for physicists: A tutorial essay on control. *Reviews of Modern Physics*, Jan 2005.

[14] J. M. Bellanger and P. Gönczy. Tac-1 and zyg-9 form a complex that promotes microtubule assembly in c. elegans embryos. *Curr Biol*, 13(17):1488–98, Sep 2003.

[15] L. D. Belmont and T. J. Mitchison. Identification of a protein that interacts with tubulin dimers and increases the catastrophe rate of microtubules. *Cell*, 84(4):623–31, Feb 1996.

[16] V. Berlin, C. A. Styles, and G. R. Fink. Bik1, a protein required for microtubule function during mating and mitosis in saccharomyces cerevisiae, colocalizes with tubulin. *The Journal of Cell Biology*, 111(6 Pt 1):2573–86, Dec 1990.

[17] P. Bieling, L. Laan, H. Schek, E. L. Munteanu, L. Sandblad, M. Dogterom, D. Brunner, and T. Surrey. Reconstitution of a microtubule plus-end tracking system in vitro. *Nature*, 450(7172):1100–5, Dec 2007.

[18] V. Bormuth, J. Howard, and E. Schäffer. Led illumination for video-enhanced dic imaging of single microtubules. *Journal of Microscopy*, Jan 2007.

[19] S. Bratman and F. Chang. Stabilization of overlapping microtubules by fission yeast clasp. *Developmental Cell*, 13(6):812–827, Dec 2007.

[20] M. V. Breugel. Stu2p, the budding yeast member of the conserved dis1/xmap215 family of microtubule-associated proteins is a plus end-binding microtubule destabilizer. *The Journal of Cell Biology*, 161(2):359–369, Apr 2003.

[21] A. L. Brittle and H. Ohkura. Mini spindles, the xmap215 homologue, suppresses pausing of interphase microtubules in drosophila. *EMBO J*, 24(7):1387–96, Apr 2005.

[22] G. J. Brouhard, J. H. Stear, T. L. Noetzel, J. Al-Bassam, K. Kinoshita, S. C. Harrison, J. Howard, and A. A. Hyman. Xmap215 is a processive microtubule polymerase. *Cell*, 132(1):79–88, Jan 2008.

[23] D. Brunner and P. Nurse. Clip170-like tip1p spatially organizes microtubular dynamics in fission yeast. *Cell*, 102(5):695–704, Sep 2000.

[24] K. E. Busch and D. Brunner. The microtubule plus end-tracking proteins mal3p and tip1p cooperate for cell-end targeting of interphase microtubules. *Curr Biol*, 14(7):548–59, Apr 2004.

[25] D. W. Buster, D. Zhang, and D. J. Sharp. Poleward tubulin flux in spindles: regulation and function in mitotic cells. *Molecular biology of the cell*, 18(8):3094–104, Aug 2007.

[26] K. A. Butner and M. W. Kirschner. Tau protein binds to microtubules through a flexible array of distributed weak sites. *J Cell Biol*, 115(3):717–30, Nov 1991.

[27] L. Cassimeris, D. Gard, P. T. Tran, and H. P. Erickson. Xmap215 is a long thin molecule that does not increase microtubule stiffness. *J Cell Sci*, 114(Pt 16):3025–33, Aug 2001.

[28] L. Cassimeris and J. Morabito. Togp, the human homolog of xmap215/dis1, is required for centrosome integrity, spindle pole organization, and bipolar spindle assembly. *Molecular biology of the cell*, 15(4):1580–90, Apr 2004.

[29] S. Charrasse, M. Schroeder, C. Gauthier-Rouviere, F. Ango, L. Cassimeris, D. L. Gard, and C. Larroque. The togp protein is a new human microtubule-associated protein homologous to the xenopus xmap215. *J Cell Sci*, 111 (Pt 10):1371–83, May 1998.

[30] D. Chrétien, I. Jáinosi, J. C. Taveau, and H. Flyvbjerg. Microtubule's conformational cap. *Cell Struct Funct*, 24(5):299–303, Oct 1999.

[31] M. Coue, V. A. Lombillo, and J. R. McIntosh. Microtubule depolymerization promotes particle and chromosome movement in vitro. *J Cell Biol*, 112(6):1165–75, Mar 1991.

[32] C. F. Cullen, P. Deák, D. M. Glover, and H. Ohkura. mini spindles: A gene encoding a conserved microtubule-associated protein required for the integrity of the mitotic spindle in drosophila. *The Journal of Cell Biology*, 146(5):1005–18, Sep 1999.

[33] P. A. Curmi, O. Gavet, E. Charbaut, S. Ozon, S. Lachkar-Colmerauer, V. Manceau, S. Siavoshian, A. Maucuer, and A. Sobel. Stathmin and its phosphoprotein family: general properties, biochemical and functional interaction with tubulin. *Cell Struct Funct*, 24(5):345–57, Oct 1999.

[34] R. Daga, A. Yonetani, and F. Chang. Asymmetric microtubule pushing forces in nuclear centering. *Current Biology*, 16(15):1544–1550, Aug 2006.

[35] A. Desai, S. Verma, T. J. Mitchison, and C. E. Walczak. Kin i kinesins are microtubule-destabilizing enzymes. *Cell*, 96(1):69–78, Jan 1999.

[36] R. Dixit, B. Barnett, J. E. Lazarus, M. Tokito, Y. E. Goldman, and E. L. F. Holzbaur. Microtubule plus-end tracking by clip-170 requires eb1. *Proc Natl Acad Sci USA*, 106(2):492–7, Jan 2009.

[37] M. Dogterom, M. Janson, C. Faivre-Moskalenko, A. van der Horst, J. Kerssemakers, C. Tanase, and B. Mulder. Force generation by polymerizing microtubules. *Applied Physics A: Materials Science & Processing*, 75(2):331–336, Aug 2002.

[38] D. Dujardin, U. I. Wacker, A. Moreau, T. A. Schroer, J. E. Rickard, and J. R. D. Mey. Evidence for a role of clip-170 in the establishment of metaphase chromosome alignment. *The Journal of Cell Biology*, 141(4):849–62, May 1998.

[39] S. Dumont and T. J. Mitchison. Force and length in the mitotic spindle. *Curr Biol*, 19(17):R749–61, Sep 2009.

[40] R. Fodde, J. Kuipers, C. Rosenberg, R. Smits, M. Kielman, C. Gaspar, J. H. van Es, C. Breukel, J. Wiegant, R. H. Giles, and H. Clevers. Mutations in the apc tumour suppressor gene cause chromosomal instability. *Nat Cell Biol*, 3(4):433–8, Apr 2001.

[41] A. D. Franck, A. F. Powers, D. R. Gestaut, T. Gonen, T. N. Davis, and C. L. Asbury. Tension applied through the dam1 complex promotes microtubule elongation providing a direct mechanism for length control in mitosis. *Nat Cell Biol*, 9(7):832–7, Jul 2007.

[42] C. T. Friel and J. Howard. The kinesin-13 mcak has an unconventional atpase cycle adapted for microtubule depolymerization. *EMBO J*, Aug 2011.

[43] M. A. Garcia, L. Vardy, N. Koonrugsa, and T. Toda. Fission yeast ch-tog/xmap215 homologue alp14 connects mitotic spindles with the kinetochore and is a component of the mad2-dependent spindle checkpoint. *EMBO J*, 20(13):3389–401, Jul 2001.

[44] D. L. Gard and M. W. Kirschner. A microtubule-associated protein from xenopus eggs that specifically promotes assembly at the plus-end. *The Journal of Cell Biology*, 105(5):2203–15, Nov 1987.

[45] M. K. Gardner, B. D. Charlebois, I. M. Jánosi, J. Howard, A. J. Hunt, and D. J. Odde. Rapid microtubule self-assembly kinetics. *Cell*, 146(4):582–92, Aug 2011.

[46] C. Gell, C. T. Friel, B. Borgonovo, D. N. Drechsel, A. A. Hyman, and J. Howard. Purification of tubulin from porcine brain. *Methods Mol Biol*, 777:15–28, Jan 2011.

[47] F. Gergely, V. M. Draviam, and J. W. Raff. The ch-tog/xmap215 protein is essential for spindle pole organization in human somatic cells. *Genes Dev*, 17(3):336–41, Feb 2003.

[48] R. A. Green and K. B. Kaplan. Chromosome instability in colorectal tumor cells is associated with defects in microtubule plus-end attachments caused by a dominant mutation in apc. *J Cell Biol*, 163(5):949–61, Dec 2003.

[49] E. L. Grishchuk, M. I. Molodtsov, F. I. Ataullakhanov, and J. R. McIntosh. Force production by disassembling microtubules. *Nature*, 438(7066):384–8, Nov 2005.

[50] M. L. Gupta, P. Carvalho, D. M. Roof, and D. Pellman. Plus end-specific depolymerase activity of kip3, a kinesin-8 protein, explains its role in positioning the yeast mitotic spindle. *Nat Cell Biol*, 8(9):913–23, Sep 2006.

[51] Y. Harada and T. Asakura. Radiation forces on a dielectric sphere in the rayleigh scattering regime. *Optics communications*, 124:529–541, Jan 1996.

[52] J. Helenius, G. Brouhard, Y. Kalaidzidis, S. Diez, and J. Howard. The depolymerizing kinesin mcak uses lattice diffusion to rapidly target microtubule ends. *Nature*, 441(7089):115–9, May 2006.

[53] G. T. Hermanson. *Bioconjugate Techniques*. Academic Press, second edition edition, May 2 2008.

[54] J. Howard and A. A. Hyman. Dynamics and mechanics of the microtubule plus end. *Nature*, 422(6933):753–8, Apr 2003.

[55] J. Howard and A. A. Hyman. Microtubule polymerases and depolymerases. *Current Opinion in Cell Biology*, 19(1):31–5, Feb 2007.

[56] B. Howell, N. Larsson, M. Gullberg, and L. Cassimeris. Dissociation of the tubulin-sequestering and microtubule catastrophe-promoting activities of oncoprotein 18/stathmin. *Molecular biology of the cell*, 10(1):105–18, Jan 1999.

[57] A. W. Hunter, M. Caplow, D. L. Coy, W. O. Hancock, S. Diez, L. Wordeman, and J. Howard. The kinesin-related protein mcak is a microtubule depolymerase that forms an atp-hydrolyzing complex at microtubule ends. *Molecular Cell*, 11(2):445–57, Feb 2003.

[58] S. Inoue, S. Satoh, M. Saito, M. Naitoh, H. Suzuki, and M. Egawa. Effects of selective vagotomy on circadian rhythms of plasma glucose, insulin and food intake in control and ventromedial hypothalamic (vmh) lesioned rats. *Obes Res*, 3 Suppl 5:747S–752S, Dec 1995.

[59] Y. H. Inoue, M. S. Savoian, T. Suzuki, E. Máthé, M.-T. Yamamoto, and D. M. Glover. Mutations in orbit/mast reveal that the central spindle is comprised of two microtubule populations, those that initiate cleavage and those that propagate furrow ingression. *The Journal of Cell Biology*, 166(1):49–60, Jul 2004.

[60] N. Instruments. Pid theory explained.

[61] K. Jiang and A. Akhmanova. Microtubule tip-interacting proteins: a view from both ends. *Current Opinion in Cell Biology*, 23(1):94–101, Feb 2011.

[62] L. Jourdain, P. Curmi, A. Sobel, D. Pantaloni, and M. F. Carlier. Stathmin: a tubulin-sequestering protein which forms a ternary t2s complex with two tubulin molecules. *Biochemistry*, 36(36):10817–21, Sep 1997.

[63] K. B. Kaplan, A. A. Burds, J. R. Swedlow, S. S. Bekir, P. K. Sorger, and I. S. Näthke. A role for the adenomatous polyposis coli protein in chromosome segregation. *Nat Cell Biol*, 3(4):429–32, Apr 2001.

[64] E. Kawamura and G. O. Wasteneys. Mor1, the arabidopsis thaliana homologue of xenopus map215, promotes rapid growth and shrinkage, and suppresses the pausing of microtubules in vivo. *J Cell Sci*, 121(Pt 24):4114–23, Dec 2008.

[65] J. W. J. Kerssemakers, E. L. Munteanu, L. Laan, T. L. Noetzel, M. E. Janson, and M. Dogterom. Assembly dynamics of microtubules at molecular resolution. *Nature*, 442(7103):709–712, Aug 2006.

[66] H. Kim, L. I. Binder, and J. L. Rosenbaum. The periodic association of map2 with brain microtubules in vitro. *J Cell Biol*, 80(2):266–76, Feb 1979.

[67] K. Kinoshita, T. L. Noetzel, L. Pelletier, K. Mechtler, D. N. Drechsel, A. Schwager, M. Lee, J. W. Raff, and A. A. Hyman. Aurora a phosphorylation of tacc3/maskin is required for centrosome-dependent microtubule assembly in mitosis. *The Journal of Cell Biology*, 170(7):1047–55, Sep 2005.

[68] K. Kita, T. Wittmann, I. S. Näthke, and C. M. Waterman-Storer. Adenomatous polyposis coli on microtubule plus ends in cell extensions can promote microtubule net growth with or without eb1. *Molecular biology of the cell*, 17(5):2331–45, May 2006.

[69] E. Kitamura, K. Tanaka, S. Komoto, Y. Kitamura, C. Antony, and T. U. Tanaka. Kinetochores generate microtubules with distal plus ends: their roles and limited lifetime in mitosis. *Developmental Cell*, 18(2):248–59, Feb 2010.

[70] Y. A. Komarova, A. S. Akhmanova, S.-I. Kojima, N. Galjart, and G. G. Borisy. Cytoplasmic linker proteins promote microtubule rescue in vivo. *The Journal of Cell Biology*, 159(4):589–99, Nov 2002.

[71] J. Kusch, A. Meyer, M. P. Snyder, and Y. Barral. Microtubule capture by the cleavage apparatus is required for proper spindle positioning in yeast. *Genes Dev*, 16(13):1627–39, Jul 2002.

[72] L. Laan, J. Husson, E. L. Munteanu, J. W. J. Kerssemakers, and M. Dogterom. Force-generation and dynamic instability of microtubule bundles. *Proc Natl Acad Sci USA*, 105(26):8920–5, Jul 2008.

[73] N. Larsson, B. Segerman, B. Howell, K. Fridell, L. Cassimeris, and M. Gullberg. Op18/stathmin mediates multiple region-specific tubulin and microtubule-regulating activities. *J Cell Biol*, 146(6):1289–302, Sep 1999.

[74] M. J. Lee, F. Gergely, K. Jeffers, S. Y. Peak-Chew, and J. W. Raff. Msps/xmap215 interacts with the centrosomal protein d-tacc to regulate microtubule behaviour. *Nat Cell Biol*, 3(7):643–9, Jul 2001.

[75] L. Mahadevan and T. J. Mitchison. Cell biology: powerful curves. *Nature*, 435(7044):895–7, Jun 2005.

[76] M. Mahamdeh. *Tweezers optimized for biological studies*. PhD thesis, Technische Universität Dresden, 2011.

[77] M. Mahamdeh and E. Schäffer. Optical tweezers with millikelvin precision of temperature-controlled objectives and base-pair resolution. *Optics express*, Jan 2009.

[78] H. Maiato, E. A. L. Fairley, C. L. Rieder, J. R. Swedlow, C. E. Sunkel, and W. C. Earnshaw. Human clasp1 is an outer kinetochore component that regulates spindle microtubule dynamics. *Cell*, 113(7):891–904, Jun 2003.

[79] H. Maiato, A. Khodjakov, and C. L. Rieder. Drosophila clasp is required for the incorporation of microtubule subunits into fluxing kinetochore fibres. *Nat Cell Biol*, 7(1):42–7, Jan 2005.

[80] T. Manna, S. Honnappa, M. O. Steinmetz, and L. Wilson. Suppression of microtubule dynamic instability by the +tip protein eb1 and its modulation by the cap-gly domain of p150glued. *Biochemistry*, 47(2):779–86, Jan 2008.

[81] T. Manna, D. Thrower, H. P. Miller, P. Curmi, and L. Wilson. Stathmin strongly increases the minus end catastrophe frequency and induces rapid treadmilling of bovine brain microtubules at steady state in vitro. *J Biol Chem*, 281(4):2071–8, Jan 2006.

[82] A. L. Manning, N. J. Ganem, S. F. Bakhoum, M. Wagenbach, L. Wordeman, and D. A. Compton. The kinesin-13 proteins kif2a, kif2b, and kif2c/mcak have distinct roles during mitosis in human cells. *Molecular biology of the cell*, 18(8):2970–9, Aug 2007.

[83] Y. Mimori-Kiyosue, I. Grigoriev, H. Sasaki, C. Matsui, A. Akhmanova, S. Tsukita, and I. Vorobjev. Mammalian clasps are required for mitotic spindle organization and kinetochore alignment. *Genes Cells*, 11(8):845–57, Aug 2006.

[84] T. Mitchison and M. Kirschner. Dynamic instability of microtubule growth. *Nature*, 312(5991):237–42, Jan 1984.

[85] A. T. Moore, K. E. Rankin, G. von Dassow, L. Peris, M. Wagenbach, Y. Ovechkina, A. Andrieux, D. Job, and L. Wordeman. Mcak associates with the tips of polymerizing microtubules. *The Journal of Cell Biology*, 169(3):391–7, May 2005.

[86] C. A. Moores, M. Perderiset, F. Francis, J. Chelly, A. Houdusse, and R. A. Milligan. Mechanism of microtubule stabilization by doublecortin. *Molecular Cell*, 14(6):833–9, Jun 2004.

[87] C. A. Moores, M. Perderiset, C. Kappeler, S. Kain, D. Drummond, S. J. Perkins, J. Chelly, R. Cross, A. Houdusse, and F. Francis. Distinct roles of doublecortin modulating the microtubule cytoskeleton. *EMBO J*, 25(19):4448–57, Oct 2006.

[88] E. E. Morrison, B. N. Wardleworth, J. M. Askham, A. F. Markham, and D. M. Meredith. Eb1, a protein which interacts with the apc tumour suppressor, is associated with the microtubule cytoskeleton throughout the cell cycle. *Oncogene*, 17(26):3471–7, Dec 1998.

[89] M. Nakamura, X. Z. Zhou, and K. P. Lu. Critical role for the eb1 and apc interaction in the regulation of microtubule polymerization. *Curr Biol*, 11(13):1062–7, Jul 2001.

[90] I. S. Näthke, C. L. Adams, P. Polakis, J. H. Sellin, and W. J. Nelson. The adenomatous polyposis coli tumor suppressor protein localizes to plasma membrane sites involved in active cell migration. *The Journal of Cell Biology*, 134(1):165–79, Jul 1996.

[91] H. Niederstrasser, H. Salehi-Had, E. C. Gan, C. Walczak, and E. Nogales. Xkcm1 acts on a single protofilament and requires the c terminus of tubulin. *J Mol Biol*, 316(3):817–28, Feb 2002.

[92] T. A. Nieminen, V. L. Y. Loke, A. B. Stilgoe, G. Knöner, A. M. Branczyk, N. R. Heckenberg, and H. Rubinsztein-Dunlop. Optical tweezers computational toolbox. *J. Opt. A: Pure Appl. Opt.*, 9:S196–S203, Jan 2007.

[93] P. Niethammer, I. Kronja, S. Kandels-Lewis, S. Rybina, P. Bastiaens, and E. Karsenti. Discrete states of a protein interaction network govern interphase and mitotic microtubule dynamics. *PLoS Biol*, 5(2):e29, Feb 2007.

[94] F. Oosawa. Size distribution of protein polymers. *J Theor Biol*, 27(1):69–86, Apr 1970.

[95] P. Pierre, J. Scheel, J. E. Rickard, and T. E. Kreis. Clip-170 links endocytic vesicles to microtubules. *Cell*, 70(6):887–900, Sep 1992.

[96] A. F. Powers, A. D. Franck, D. R. Gestaut, J. Cooper, B. Gracyzk, R. R. Wei, L. Wordeman, T. N. Davis, and C. L. Asbury. The ndc80 kinetochore complex forms load-bearing attachments to dynamic microtubule tips via biased diffusion. *Cell*, 136(5):865–75, Mar 2009.

[97] N. K. Pryer, R. A. Walker, V. P. Skeen, B. D. Bourns, M. F. Soboeiro, and E. D. Salmon. Brain microtubule-associated proteins modulate microtubule dynamic

instability in vitro. real-time observations using video microscopy. *J Cell Sci*, 103 (Pt 4):965–76, Dec 1992.

[98] R. B. G. Ravelli, B. Gigant, P. A. Curmi, I. Jourdain, S. Lachkar, A. Sobel, and M. Knossow. Insight into tubulin regulation from a complex with colchicine and a stathmin-like domain. *Nature*, 428(6979):198–202, Mar 2004.

[99] J. E. Rickard and T. E. Kreis. Identification of a novel nucleotide-sensitive microtubule-binding protein in hela cells. *The Journal of Cell Biology*, 110(5):1623–33, May 1990.

[100] B. Rockmill and S. Fogel. Dis1: a yeast gene required for proper meiotic chromosome disjunction. *Genetics*, 119(2):261–72, Jun 1988.

[101] S. L. Rogers, G. C. Rogers, D. J. Sharp, and R. D. Vale. Drosophila eb1 is important for proper assembly, dynamics, and positioning of the mitotic spindle. *The Journal of Cell Biology*, 158(5):873–84, Sep 2002.

[102] T. Savin and P. S. Doyle. Static and dynamic errors in particle tracking microrheology. *Biophys J*, 88(1):623–38, Jan 2005.

[103] E. Schäffer, S. Nørrelykke, and J. Howard. Surface forces and drag coefficients of microspheres near a plane surface measured with optical tweezers. *Langmuir*, 23:3654–3665, Jan 2007.

[104] H. Schek, M. Gardner, J. Cheng, D. Odde, and A. Hunt. Microtubule assembly dynamics at the nanoscale. *Current Biology*, 17(17):1445–1455, Sep 2007.

[105] J. G. Skellam. The frequency distribution of the difference between two poisson variates belonging to different populations. *J R Stat Soc Ser A*, 109(Pt 3):296, Jan 1946.

[106] K. C. Slep and R. D. Vale. Structural basis of microtubule plus end tracking by xmap215, clip-170, and eb1. *Molecular Cell*, 27(6):976–91, Sep 2007.

[107] K. J. Smith, D. B. Levy, P. Maupin, T. D. Pollard, B. Vogelstein, and K. W. Kinzler. Wild-type but not mutant apc associates with the microtubule cytoskeleton. *Cancer Res*, 54(14):3672–5, Jul 1994.

[108] C. Spittle, S. Charrasse, C. Larroque, and L. Cassimeris. The interaction of togp with microtubules and tubulin. *J Biol Chem*, 275(27):20748–53, Jul 2000.

[109] L. R. Sproul, D. J. Anderson, A. T. Mackey, W. S. Saunders, and S. P. Gilbert. Cik1 targets the minus-end kinesin depolymerase kar3 to microtubule plus ends. *Curr Biol*, 15(15):1420–7, Aug 2005.

[110] M. O. Steinmetz, R. A. Kammerer, W. Jahnke, K. N. Goldie, A. Lustig, and J. van Oostrum. Op18/stathmin caps a kinked protofilament-like tubulin tetramer. *EMBO J*, 19(4):572–80, Feb 2000.

[111] K. Tanaka, N. Mukae, H. Dewar, M. van Breugel, E. K. James, A. R. Prescott, C. Antony, and T. U. Tanaka. Molecular mechanisms of kinetochore capture by spindle microtubules. *Nature*, 434(7036):987–94, Apr 2005.

[112] J. S. Tirnauer, S. Grego, E. D. Salmon, and T. J. Mitchison. Eb1-microtubule interactions in xenopus egg extracts: role of eb1 in microtubule stabilization and mechanisms of targeting to microtubules. *Molecular biology of the cell*, 13(10):3614–26, Oct 2002.

[113] J. S. Tirnauer, E. O'Toole, L. Berrueta, B. E. Bierer, and D. Pellman. Yeast bim1p promotes the g1-specific dynamics of microtubules. *The Journal of Cell Biology*, 145(5):993–1007, May 1999.

[114] C. Tischer, D. Brunner, and M. Dogterom. Force- and kinesin-8-dependent effects in the spatial regulation of fission yeast microtubule dynamics. *Mol Syst Biol*, 5:250, Jan 2009.

[115] S. Tolić-Nørrelykke, E. Schäffer, J. Howard, and F. Jülicher. Calibration of optical tweezers with positional detection in the back focal plane. *Rev. Sci. Instrum*, 77(103101), Jan 2006.

[116] R. Tournebize, A. Popov, K. Kinoshita, A. J. Ashford, S. Rybina, A. Pozniakovsky, T. U. Mayer, C. E. Walczak, E. Karsenti, and A. A. Hyman. Control of microtubule dynamics by the antagonistic activities of xmap215 and xkcm1 in xenopus egg extracts. *Nat Cell Biol*, 2(1):13–9, Jan 2000.

[117] P. T. Tran, L. Marsh, V. Doye, S. Inoué, and F. Chang. A mechanism for nuclear positioning in fission yeast based on microtubule pushing. *The Journal of Cell Biology*, 153(2):397–411, Apr 2001.

[118] C. L. Troxell, M. A. Sweezy, R. R. West, K. D. Reed, B. D. Carson, A. L. Pidoux, W. Z. Cande, and J. R. McIntosh. pkl1(+)and klp2(+): Two kinesins of the kar3 subfamily in fission yeast perform different functions in both mitosis and meiosis. *Molecular biology of the cell*, 12(11):3476–88, Nov 2001.

[119] M. van Breugel, D. Drechsel, and A. Hyman. Stu2p, the budding yeast member of the conserved dis1/xmap215 family of microtubule-associated proteins is a plus end-binding microtubule destabilizer. *The Journal of Cell Biology*, 161(2):359–69, Apr 2003.

[120] A. Vandecandelaere, B. Pedrotti, M. A. Utton, R. A. Calvert, and P. M. Bayley. Differences in the regulation of microtubule dynamics by microtubule-associated proteins map1b and map2. *Cell Motil Cytoskeleton*, 35(2):134–46, Jan 1996.

[121] V. Varga, J. Helenius, K. Tanaka, A. A. Hyman, T. U. Tanaka, and J. Howard. Yeast kinesin-8 depolymerizes microtubules in a length-dependent manner. *Nat Cell Biol*, 8(9):957–62, Sep 2006.

[122] B. Vitre, F. M. Coquelle, C. Heichette, C. Garnier, D. Chrétien, and I. Arnal. Eb1 regulates microtubule dynamics and tubulin sheet closure in vitro. *Nat Cell Biol*, 10(4):415–21, Apr 2008.

[123] P. J. Wang and T. C. Huffaker. Stu2p: A microtubule-binding protein that is an essential component of the yeast spindle pole body. *The Journal of Cell Biology*, 139(5):1271–80, Dec 1997.

[124] A. T. Whittington, O. Vugrek, K. J. Wei, N. G. Hasenbein, K. Sugimoto, M. C. Rashbrooke, and G. O. Wasteneys. Mor1 is essential for organizing cortical microtubules in plants. *Nature*, 411(6837):610–3, May 2001.

[125] P. O. Widlund, J. H. Stear, A. Pozniakovsky, M. Zanic, S. Reber, G. J. Brouhard, A. A. Hyman, and J. Howard. Xmap215 polymerase activity is built by combining multiple tubulin-binding tog domains and a basic lattice-binding region. *Proc Natl Acad Sci USA*, 108(7):2741–6, Feb 2011.

[126] T. Wittmann, G. M. Bokoch, and C. M. Waterman-Storer. Regulation of microtubule destabilizing activity of op18/stathmin downstream of rac1. *J Biol Chem*, 279(7):6196–203, Feb 2004.

[127] M. J. Wolyniak, K. Blake-Hodek, K. Kosco, E. Hwang, L. You, and T. C. Huffaker. The regulation of microtubule dynamics in saccharomyces cerevisiae by three interacting plus-end tracking proteins. *Molecular biology of the cell*, 17(6):2789–98, Jun 2006.

[128] L. Wordeman and T. J. Mitchison. Identification and partial characterization of mitotic centromere-associated kinesin, a kinesin-related protein that associates with centromeres during mitosis. *The Journal of Cell Biology*, 128(1-2):95–104, Jan 1995.

[129] E. Yeh, C. Yang, E. Chin, P. Maddox, E. D. Salmon, D. J. Lew, and K. Bloom. Dynamic positioning of mitotic spindles in yeast: role of microtubule motors and cortical determinants. *Molecular biology of the cell*, 11(11):3949–61, Nov 2000.

[130] J. Zumbrunn, K. Kinoshita, A. A. Hyman, and I. S. Näthke. Binding of the adenomatous polyposis coli protein to microtubules increases microtubule stability and is regulated by gsk3 beta phosphorylation. *Curr Biol*, 11(1):44–9, Jan 2001.

Acknowledgments

I would like to thank to Prof. Dr. Joe Howard for my exciting project, for his support and motivation during the course of this work. I am deeply grateful to Dr. Erik Schäffer for all his efforts in supervising this work and for patient reviewing my thesis.

I am grateful to Volker Bormuth for teaching me optical tweezers techniques, his help and warm encouragement. Special thanks I want to say to Marija Žanić for the fruitful scientific discussion and reviewing my thesis.

I thank all members of Howard group, especially Marija Žanić, Joshua Alper, Horatiu Fantana, Veikko Geyer, Marko Storch, Marija Podolski,Vikram Mukundan, former members of Howard group Clair Friel and Chris Gell for the scientific discussion, constructive critic, their involvement and support. I am also grateful to all members of Howard group for creation of friendly and heartwarming atmosphere in the lab. Special thanks I would like to say to Nanomechanics group for their help and support, especially Deepikaa Menon, Anita Jannasch and Mohammed Mahamdeh.

I want to say thanks to Per Widlund for teaching me XMAP215 purification. I am grateful to Protein expression and purification facility, especially Régis Lemaitre and Barbara Borgonovo for helping me with XMAP215 expression and purification. I thank Heike Petzold for teaching me the basics of molecular cloning.

And last but not least, I would like to thanks to my family and friends for their support and friendship we share.

Declaration

Erklärung entsprechend § 5.5 der Promotionsordnung

Hiermit versichere ich, dass ich die vorliegende Arbeit ohne unzulässige Hilfe Dritter und ohne Benutzung anderer als der angegebenen Hilfsmittel angefertigt habe; die aus fremden Quellen direkt oder indirekt übernommenen Gedanken sind als solche kenntlich gemacht. Die Arbeit wurde bisher weder im Inland noch im Ausland in gleicher oder ähnlicher Form einer anderen Prfungsbehörde vorgelegt.
Die Dissertation wurde im Zeitraum vom 1.11.2007 bis 22.12.2011 verfasst und von Prof. Dr. Jonathan Howard, Max Planck Institute of Cell Molecular Biology and Genetics, Howard group betreut.
Meine Person betreffend erkläre ich hiermit, dass keine früheren erfolglosen Promotionsverfahren stattgefunden haben.
Ich erkenne die Promotionsordnung der Fakultät für Mathematik und Naturwissenschaften, Technische Universität Dresden an.

Declaration according to § 5.5 of the doctorate regulations

I herewith declare that I have produced this paper without the prohibited assistance of third parties and without making use of aids other than those specified; notions taken over directly or indirectly from other sources have been identified as such. This paper has not previously been presented in identical or similar form to any other German or foreign examination board.
The thesis work was conducted from starting date to date of finish under the supervision of Prof. Dr. Jonathon Howard at Max Planck Institute of Molecular Cell Biology and Genetics, Howard group. I declare that I have not undertaken any previous unsuccessful doctorate proceedings. I declare that I recognize the doctorate regulations of the Fakultät für Mathematik und Naturwissenschaften of the Technische Universität Dresden.

Date_____ Signature_____